ATLAS NOTE

ATL-PHYS-PUB-2016-020

16th October 2017

Studies on top-quark Monte Carlo modelling for Top2016

The ATLAS Collaboration

Abstract

This note summarises recent studies on Monte Carlo simulation setups of top-quark pair production used by the ATLAS experiment and presents a new method to deal with interference effects for the *Wt* single-top-quark production which is compared against previous techniques. The main focus for the top-quark pair production is on the improvement of the modelling of the POWHEG generator interfaced to the PYTHIA8 and HERWIG7 shower generators. The studies are done using unfolded data at centre-of-mass energies of 7, 8, and 13 TeV.

The following have been revised with respect to the version dated September 15, 2016: the chosen values of the main31 parameters were corrected in Section 2.2.2, and Eq. (3) was modified due to a typing error.

The following have been revised with respect to the version dated September 16, 2016: the number of additional jets produced at NLO accuracy in the Sherpa 2.2 ttbar sample was clarified in Section 2.

ATL-PHYS-PUB-2016-020
18/10/2017

1 Introduction

The LHC has been successfully running at a centre-of-mass energy of $\sqrt{s}$ = 13 TeV and collected as much data as in Run-1 at $\sqrt{s}$ = 8 TeV. Several Run-1 and Run-2 measurements and searches have been performed involving top-quark processes using the ATLAS detector. In the majority of these analyses, the systematic uncertainties associated with the top-quark-physics modelling are among those which have the largest impact on the final results. Furthermore, top-quark pairs can decay to a variety of possible topologies involving jets, charged leptons and missing transverse momentum in the final state. Therefore, given the large inclusive production cross-section, top-quark pair ($t\bar{t}$) events contribute sizeable backgrounds to a number of analyses such as Higgs physics, SUSY searches and Standard Model measurements.

The ATLAS Collaboration has previously documented the choice of Monte Carlo (MC) generator parameters and the testing of new MC setups in order to improve the description of top-quark physics [1–3]. The aim of this note is to present new studies that further improve the modelling of data through development of new MC generator configurations. Two topics are presented in this note: the optimisation of Powheg+Pythia8 and Powheg+Herwig7 for modelling top-quark pair production and a study of a new technique to approximate the interference effects between top-quark pair and single top-quark production. Section 2 describes studies which make use of $\sqrt{s}$ = 7 TeV and $\sqrt{s}$ = 8 TeV measurements to improve the MC generator configurations and the modelling they provide of top-quark pair production that is available for use in ATLAS analyses The proposed improved settings are also compared to the first measurements at $\sqrt{s}$ = 13 TeV and with alternative generator setups. Section 3 presents the implementation of a new diagram removal scheme to deal with the overlap between $t\bar{t}$ and the associated production of single-top-quarks with one or two gauge bosons. Comparisons of the new scheme against existing schemes are shown and discussed. The conclusions of this note are then summarised in Section 4.

2 Studies of $t\bar{t}$ production

A range of $t\bar{t}$ MC generators are currently available, and the MC generator configurations that will be studied in this note are summarised in Table 1. While leading-order (LO) precision predictions are also available for ATLAS analyses, this note focuses on samples with next-to-leading order (NLO) precision in the strong coupling. The $t\bar{t}$ inclusive production cross-sections are corrected to the prediction at next-to-next-to-leading order (NNLO) in QCD including the resummation of next-to-next-to-leading logarithmic (NNLL) soft-gluon terms calculated using Top++2.0 [4–10][1]. For proton–proton collisions at $\sqrt{s} = 13$ TeV, this cross section corresponds to $\sigma(t\bar{t})_{\text{NNLO+NNLL}} = 831.8 \pm 51.2$ fb.

So far, the most commonly used $t\bar{t}$ sample in recent ATLAS analyses is generated using Powheg [11, 12] interfaced to Pythia6 [13] with the Perugia set of tunable parameters [14]. In this sample, the PDF used in the matrix element (ME) calculation is CT10 [15] and the PDF used in the parton shower (PS) is CTEQ6L1 [16]. For the studies presented in this note, new $t\bar{t}$ samples were generated using Powheg interfaced with Pythia8 [17] using the A14 set of tunable parameters [18] or with Herwig7 [19, 20] using the H7UE set of tunable parameters [20]. In addition to Powheg, an NLO inclusive sample is produced with MadGraph5_aMC@NLO [21] interfaced to Pythia8 using the A14 set of tunable parameters. This sample makes use of the NNPDF [22, 23] PDF sets, using NNPDF3.0 in the ME and NNPDF2.3 in the PS. Additionally, top-quark spin correlations are preserved through the use of MadSpin [24].

Along with the various inclusive NLO $t\bar{t}$ samples described above, additional samples are studied which are offering higher precision through the use of state-of-the-art matching and merging prescriptions, and using the prescriptions based on the studies reported in [3]. These samples improve the accuracy of observables which are formally described to leading-log (LL) precision by the PS in inclusive NLO samples. A Sherpa 2.2 [25] sample is studied which implements the MEPS@NLO matching scheme [26] interfaced to the Sherpa 2.2 parton shower and provides NLO precision for observables of one additional jet and LO precision for the second, third, and fourth additional jets. In addition a MadGraph5_aMC@NLO sample is studied which implements the FxFx matching scheme [27] interfaced to Pythia8 and can provide NLO precision for observables of one or two additional jets. These samples make use of the NNPDF PDF sets in the ME and in the PS which also improves the top-quark kinematic description, particularly improving the top-quark rapidity [2].

[1] NLO electroweak corrections are not taken into account in this study.

ME Gen.	**PS/UE Gen.**	**ME** **PS/UE PDF**	**PS Tune**	**Matching** (**Merging**)
Powheg-Box r2330.3	Pythia 6.427	CT10 CTEQ6L1	P2012	Powheg ($h_{\text{damp}} = m_{\text{top}}$)
Powheg-Box r3026 (v2)	Pythia 8.210	NNPDF3.0NLO NNPDF2.3LO	A14	Powheg ($h_{\text{damp}} = 0.5\text{-}2.0\ m_{\text{top}}$)
Powheg-Box r2330.3	Herwig 7.0.1	CT10 MMHT2014lo68cl	H7-UE-MMHT	Powheg
MadGraph5_aMC@NLO 2.3.3	Pythia 8.212	NNPDF3.0NLO NNPDF2.3LO	A14	MC@NLO
MadGraph5_aMC@NLO 2.3.3	Pythia 8.210	NNPDF3.0NLO NNPDF2.3LO	A14	MC@NLO (FxFx, μ_Q = 70 GeV)
Sherpa 2.2	Sherpa	NNPDF3.0NNLO	Default	MC@NLO (MEPS@NLO, Q = 30 GeV)

Table 1: ME and PS/UE generator settings for each of the MC samples used for the studies presented in this note. The generator versions, the PDFs used for the ME and in the PS and the matching scheme are shown alongside the tune.

2.1 Measurements of $t\bar{t}$ production

Predictions of various MC generators are compared to ATLAS data. Unfolded distributions from 7 TeV, 8 TeV, and 13 TeV measurements are taken into account. Compared to previous studies based on 7 TeV data [1–3], the 8 TeV measurements have smaller uncertainties and allow for a better comparison. Measurements are unfolded either to particle level in a fiducial phase-space or at parton level in the full phase-space. Particle-level objects are defined for simulated events in analogy to detector-level objects. Only stable final-state particles, i.e. particles with a mean lifetime $\tau > 300$ ps are considered. Parton level top quarks are taken at the point after the top quark has emitted any QCD radiation, but before it decays. The studies shown in this document have been performed with Rivet v.2.4.0 [28] and the analyses used are listed below.

- **Analysis A: Measurement of top-quark pair differential cross-sections in the lepton+jets channel in pp collisions at $\sqrt{s}$ = 8 TeV using the ATLAS detector (not yet published in Rivet) [29]**

  The cross-sections are measured at stable particle level and at parton level as a function of the transverse momentum and absolute rapidity of the hadronically decaying top quark and as a function of the transverse momentum, absolute rapidity and invariant mass of the $t\bar{t}$-system. The events are selected in the lepton+jets channel, which is characterised by the presence of exactly one charged lepton (electron or muon), at least four jets with at least two jets being identified to originate from a b-quark. Jets originating from b-quarks are defined using a B-hadron matching, requiring at least one B-hadron to be found within the jet using the ghost association technique [30–32]. The jets are reconstructed with the anti-k_t jet algorithm with a radius parameter $R = 0.4$ [33]. Only jets with $p_{\mathrm{T}} > 25$ GeV and $|\eta| < 2.5$ are considered in the analysis. The results are defined at truth particle level and are corrected for all detector effects, within a kinematic range closely matched to the experimental acceptance. The data used in this measurement were taken with the ATLAS experiment at $\sqrt{s} = 8$ TeV.

- **Analysis B: Measurement of the differential cross-section of highly boosted top quarks as a function of their transverse momentum in $\sqrt{s}$ = 8 TeV proton-proton collisions using the ATLAS detector (Rivet analysis: ATLAS_2015_I1397637) [34]**

  The cross-section is measured at stable particle level as a function of the transverse momentum of the hadronically decaying top quark with $p_{\mathrm{T}} > 300$ GeV. The events are selected in the lepton+jets channel, which is characterised by the presence of exactly one charged lepton (electron or muon), at least one small-R jet close to the lepton ($\Delta R < 1.5$) and one large-R jet with $p_{\mathrm{T}} > 300$ GeV and $m > 100$ GeV. Additional cuts on the large-R jet substructure are applied to identify it to originate from a top quark, which is required to be well separated from the lepton and the small-R jet. At least one jet within the large-R jet or the jet close to the lepton candidate have to be identified to originate from a b-quark. The small-R jets are reconstructed with the anti-k_t jet algorithm with a radius parameter $R = 0.4$ [33]. Only jets with $p_{\mathrm{T}} > 25$ GeV and $|\eta| < 2.5$ are considered in the analysis. Events are selected if they satisfy a requirement on the missing transverse momentum ($E_{\mathrm{T}}^{\mathrm{miss}}$) and on the transverse mass[2] $m_{\mathrm{T}}(\ell, E_{\mathrm{T}}^{\mathrm{miss}})$: $E_{\mathrm{T}}^{\mathrm{miss}} > 20$ GeV and $E_{\mathrm{T}}^{\mathrm{miss}} + m_{\mathrm{T}}(\ell, E_{\mathrm{T}}^{\mathrm{miss}}) > 60$ GeV. The large-R jets are reconstructed with a radius parameter of $R = 1.0$. The leading large-R jet which is identified to originate from a top quark is used as hadronic top-quark candidate. The results are defined at truth particle level and are corrected for all detector effects, within a kinematic range closely matched to

[2] The transverse mass $m_{\mathrm{T}}(\ell, E_{\mathrm{T}}^{\mathrm{miss}})$ of the lepton and the $E_{\mathrm{T}}^{\mathrm{miss}}$ is defined as $m_{\mathrm{T}}(\ell, E_{\mathrm{T}}^{\mathrm{miss}}) = \sqrt{2p_{\mathrm{T}}^{\ell} E_{\mathrm{T}}^{\mathrm{miss}}(1 - \cos\Delta\phi)}$, where p_{T}^{ℓ} is the lepton transverse momentum and $\Delta\phi$ the azimuthal difference between the lepton and the $E_{\mathrm{T}}^{\mathrm{miss}}$.

the experimental acceptance. The same analysis also provides unfolded distributions of top-quark and $t\bar{t}$ observables on parton level. The data used in this measurement were taken with the ATLAS experiment at $\sqrt{s} = 8$ TeV.

- **Analysis C: Measurements of top-quark pair differential cross-sections in the lepton+jets channel in pp collisions at $\sqrt{s} = 13$ TeV using the ATLAS detector (not yet published in Rivet) [35]**

  The cross-sections are measured at stable particle level in the resolved and the boosted topology. In the resolved topology, the observables are the transverse momentum and absolute rapidity of the hadronically decaying top quark as well as the the transverse momentum, absolute rapidity and invariant mass of the $t\bar{t}$-system. The events are selected in the lepton+jets channel, which is characterised by the presence of exactly one charged lepton (electron or muon), at least four jets with at least two jets being identified to originate from a b-quark using the same technique described in Analysis A. The jets are reconstructed with the anti-k_t jet algorithm with a radius parameter $R = 0.4$ [33]. Only jets with $p_{\mathrm{T}} > 25$ GeV and $|\eta| < 2.5$ are considered in the analysis. The results are defined at truth particle level and are corrected for all detector effects, within a kinematic range closely matched to the experimental acceptance. The data used in this measurement were taken with the ATLAS experiment at $\sqrt{s} = 13$ TeV.

- **Analysis D: Measurements of normalized differential cross-sections for $t\bar{t}$ production in pp collisions at $\sqrt{s} = 7$ TeV using the ATLAS detector (not published in Rivet) [36]**

  Differential cross-sections for top-quark pair-production are measured as a function of the top-quark p_{T}, and of the mass, p_{T}, and rapidity of the $t\bar{t}$ system. Events are selected in the lepton+jets channel, requiring exactly one lepton and at least four jets with at least one of the jets tagged as originating from a b-quark. Jets are reconstructed using the anti-k_t jet algorithm with a radius parameter $R = 0.4$ [33] and are required to have $p_{\mathrm{T}} > 25$ GeV and $|\eta| < 2.5$. The top-quark and top-antiquarks are reconstructed from the reconstructed jets, leptons and missing transverse momentum. The distributions are unfolded to the parton level, corresponding to the point after the top quark has emitted any QCD radiation, but before it decays. The data used in this measurement were taken with the ATLAS experiment at $\sqrt{s} = 7$ TeV.

- **Analysis E: Measurement of the $t\bar{t}$ production cross-section as a function of jet multiplicity and jet transverse momentum in 7 TeV pp collisions with the ATLAS detector (Rivet analysis: ATLAS_2014_I1304688) [37]**

  The differential cross-sections are measured as a function of the jet multiplicity for up to eight jets using jet transverse momentum thresholds of 25, 40, 60, and 80 GeV, and as a function of jet transverse momentum up to the fifth leading jet. The events are selected in the lepton+jets channel, requiring exactly one lepton and at least three jets with at least one of the jets tagged as originating from a b-quark using the same technique described in Analysis A. Jets are reconstructed using the anti-k_t jet algorithm with a radius parameter $R = 0.4$ [33] and are required to have $p_{\mathrm{T}} > 25$ GeV and $|\eta| < 2.5$. The results are defined at truth particle level and are corrected for all detector effects, within a kinematic range closely matched to the experimental acceptance. The data used in this measurement were taken with the ATLAS experiment at $\sqrt{s} = 7$ TeV.

- **Analysis F: Measurements of fiducial cross-sections for $t\bar{t}$ production with one or two additional b-jets in pp collisions at $\sqrt{s} = 8$ TeV using the ATLAS detector (Rivet analysis: ATLAS_2015_I1390114) [38]**

The fiducial cross-sections of $t\bar{t}$ plus one additional b-jet ($t\bar{t}$ +b) has been measured in the lepton+jets and dilepton channel and the fiducial cross-section of $t\bar{t}$ plus two additional b-jets ($t\bar{t}$ +bb) has been measured in the dilepton channel. The ratio of cross-sections between $t\bar{t}$ plus two b-jets and $t\bar{t}$ plus two additional jets has also been extracted from the data. The events are selected in the lepton+jets channel by requiring exactly one charged lepton (electron or muon) with $p_{\mathrm{T}} > 20\,\mathrm{GeV}$ and $|\eta| < 2.5$ and at least four jets. Jets are reconstructed using the anti-k_t jet algorithm with a radius parameter $R = 0.4$ and are required to have $p_{\mathrm{T}} > 25\,\mathrm{GeV}$ and $|\eta| < 2.5$. The events are also selected in the dilepton channel by requiring exactly two leptons with $p_{\mathrm{T}} > 20\,\mathrm{GeV}$ and $|\eta| < 2.5$ and at least two jets. The number of b-tagged jets is dependent on the cross-section being measured, with at least three b-tagged jets required for $t\bar{t}$ +b measurements and at least four b-tagged jets required for the $t\bar{t}$ +bb measurement. The ghost association technique [30–32] is used to estimate templates of $t\bar{t}$ with additional jets, split by the number of heavy flavour hadrons present in the additional jets, for use in the fit-based cross-section measurements. The data used in this measurement were taken with the ATLAS experiment at $\sqrt{s} = 8\,\mathrm{TeV}$.

2.2 Optimisation studies for POWHEG+PYTHIA8

Studies have been performed on the optimisation of the parameters of POWHEG+PYTHIA8 following on from the studies presented in [2]. Here the focus is on choosing the optimal POWHEG h_{damp} parameter. This parameter is used as a resummation damping factor, which is one of the parameters controlling the ME/PS matching in POWHEG and effectively regulates the high-p_{T} radiation. The default POWHEG+PYTHIA6 sample used $h_{\text{damp}} = m_{\text{top}}$ and the current POWHEG+PYTHIA8 sample used the same h_{damp} value.

In addition to the POWHEG h_{damp} parameter, there are parameters in the `main31` PYTHIA8 routine which control the merging between POWHEG and PYTHIA8 through the use of vetoed showering. This allows PYTHIA8 to shower the full phase-space, while vetoing emissions. Two parameters of interest are `pTdef`, which controls whether the p_{T} is defined by POWHEG or by PYTHIA8, and `pThard`, which controls the shower veto scale definition.

The description of unfolded measurements while varying h_{damp} between 0.5 and 2.0 times m_{top} is presented in this section. This h_{damp} range was selected after comparing the description of data with a larger range of values and finding that h_{damp} greater than two times the top mass does not adequately describe the data. The impact of different `pTdef` and `pThard` options is also studied and compared to unfolded measurements.

2.2.1 Optimisation of h_{damp}

The 8 TeV resolved analysis (Analysis A) provides more precise top quark kinematic measurements than those made with the 7 TeV dataset which allows for comparing finer variations of h_{damp} to data than has previously been performed. Four samples have been produced with different h_{damp} values. Defining $h_{\text{damp}} = h \cdot m_{\text{top}}$, the four samples have been generated with $h = [0.5, 1.0, 1.5, 2.0]$. The distributions used to optimise the h_{damp} parameter are those which are sensitive to additional radiation in the $t\bar{t}$ system. Two key variables are the transverse momentum of the $t\bar{t}$ system ($p_T^{t\bar{t}}$) and the out-of-plane momentum ($|p_{\text{out}}^{t\bar{t}}|$) of the hadronically decaying top quark ($\vec{p}_{t,\text{had}}$) with respect to the plane defined by the leptonically decaying top quark ($\vec{p}_{t,\text{lep}}$) and the beamline ($\hat{z}$):

$$|p_{\text{out}}^{t\bar{t}}| = \left|\vec{p}_{t,\text{had}} \cdot \frac{\vec{p}_{t,\text{lep}} \times \hat{z}}{|\vec{p}_{t,\text{lep}} \times \hat{z}|}\right|. \tag{1}$$

These distributions are shown in Fig. 1 for the resolved regime, where separation between the samples with different h_{damp} values can be observed. The invariant mass of the top-quark pair ($m_{t\bar{t}}$) and the transverse momentum of the hadronically decaying top-quark ($p_T^{t,\text{had}}$) are less sensitive to the value of h_{damp} and are also presented to show that the top-quark kinematics are not adversely affected by tuning h_{damp}. The transverse momentum of the top-jet candidate in the boosted regime (Analysis B) is shown in Fig. 2 and checked to ensure that the boosted top-quark kinematics are not affected by changing h_{damp}. It is clear from these plots that a h_{damp} value smaller than m_{top} is strongly disfavoured by the data. From these distributions, the data appears to be best described using $h_{\text{damp}} = 1.5 \cdot m_{\text{top}}$ or $h_{\text{damp}} = 2.0 \cdot m_{\text{top}}$. Similar distributions have been produced using the 13 TeV measurements from Analysis C and are shown in Fig. 3. In these distributions the data is best described using $h_{\text{damp}} = 1.0 \cdot m_{\text{top}}$ or $h_{\text{damp}} = 1.5 \cdot m_{\text{top}}$. Therefore, to offer the best agreement between multiple centre-of-mass energies, using $h_{\text{damp}} = 1.5 \cdot m_{\text{top}}$ is the preferred value.

This value of h_{damp} has been checked against the 7 TeV measurements which were used to determine the original h_{damp} tuning performed by ATLAS [1, 2] with Analysis D. The 7 TeV data can be seen in Fig. 4 to be described by both $h_{\text{damp}} = 1.0 \cdot m_{\text{top}}$ and $h_{\text{damp}} = 1.5 \cdot m_{\text{top}}$. As such, there is no conflict between the h_{damp} tuning performed for Run-1 and this new tuning performed for Run-2.

The effect of the h_{damp} parameter on the jet multiplicity and on the jet transverse momenta has been checked using 7 TeV data (Analysis E), as shown in Fig. 5. Both $h_{\text{damp}} = 1.0 \cdot m_{\text{top}}$ and $h_{\text{damp}} = 1.5 \cdot m_{\text{top}}$ give good modelling of the unfolded distributions, given the experimental uncertainties.

Finally, the effect of the h_{damp} parameter on the additional b-jet production has been checked using 8 TeV data (Analysis F), as shown in Fig. 6. The large uncertainties on the experimental measurement do not permit to assess which setting is favoured by the unfolded data of this analysis, but the cross-sections in the fiducial regions with one or two additional b-jets are increased by setting the h_{damp} parameter to a higher value, while the the ratio of $t\bar{t}$ production with two additional b-jets to $t\bar{t}$ production with any two additional jets remains the same.

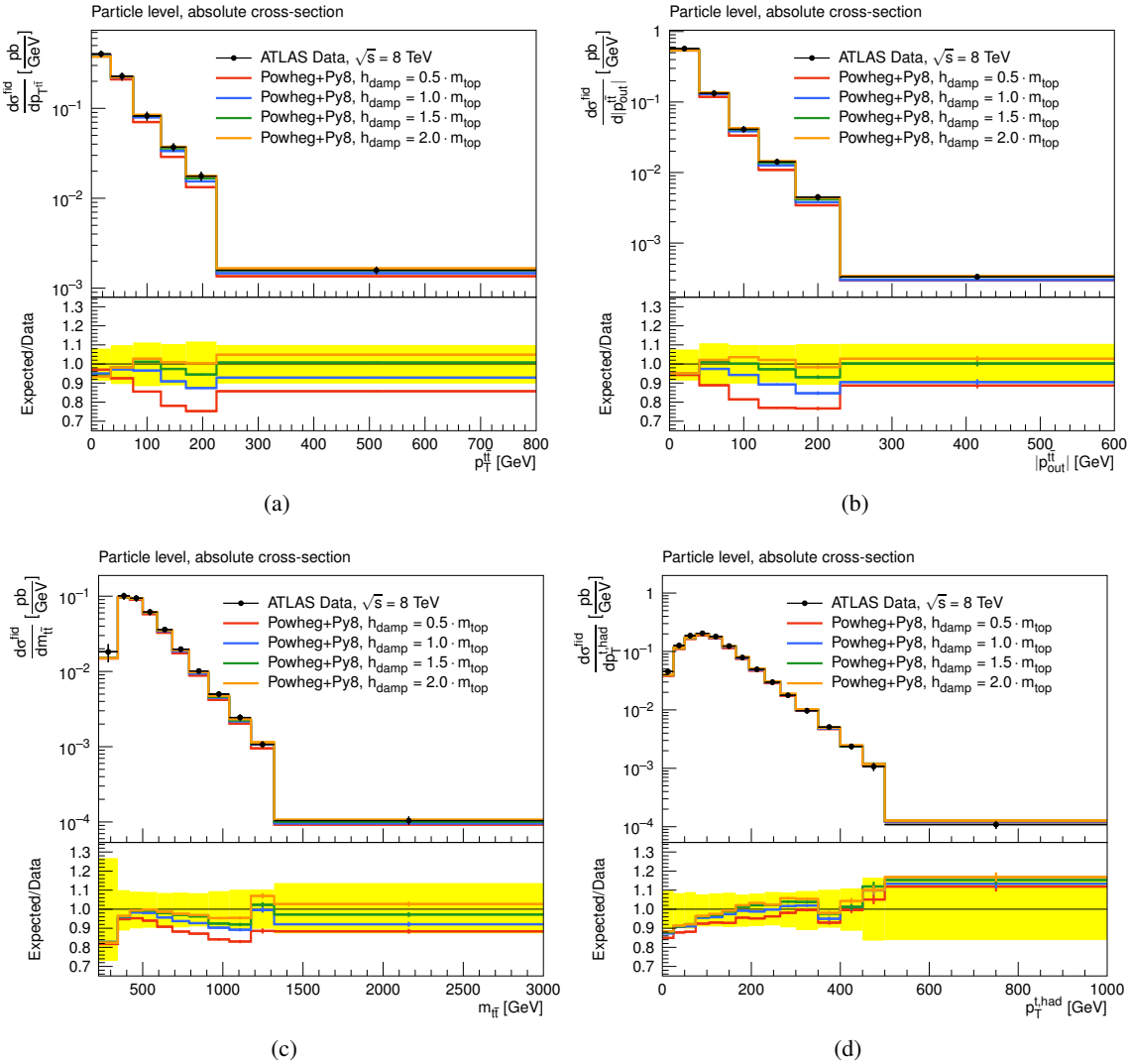

Figure 1: The POWHEG+PYTHIA8 samples with different h_{damp} variations are compared to data at $\sqrt{s}$ = 8 TeV. The comparison is performed for (a) the transverse momentum of the $t\bar{t}$ system, (b) the out-of-plane momentum, (c) the invariant mass of the $t\bar{t}$ system and (d) the transverse momentum of the hadronic top quark candidate in $t\bar{t}$ lepton+jets events (resolved channel) using ATLAS data unfolded to particle level in Analysis A [29]. The data are represented as closed (black) circles with statistical uncertainties. The yellow band is the total experimental uncertainty on the data (statistical and systematic). The generator predictions are shown as solid colored lines.

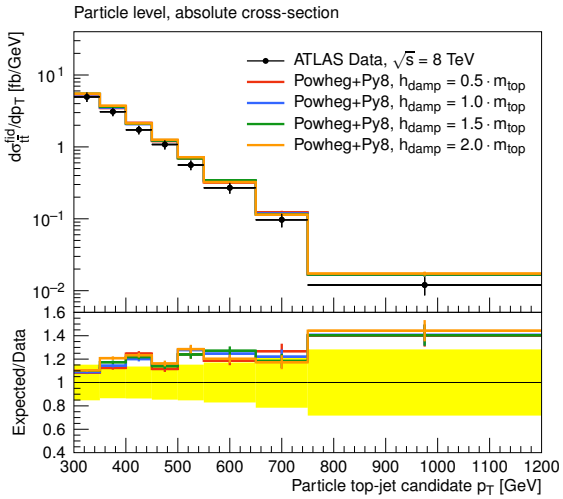

Figure 2: The Powheg+Pythia8 samples with different h_{damp} variations are compared to data at $\sqrt{s} = 8$ TeV. The comparison is performed for the transverse momentum of the hadronic top-quark candidate in $t\bar{t}$ lepton+jets events (boosted channel) using ATLAS data unfolded to particle level in Analysis B [34]. The data and generator predictions are presented the same way as in Fig. 1.

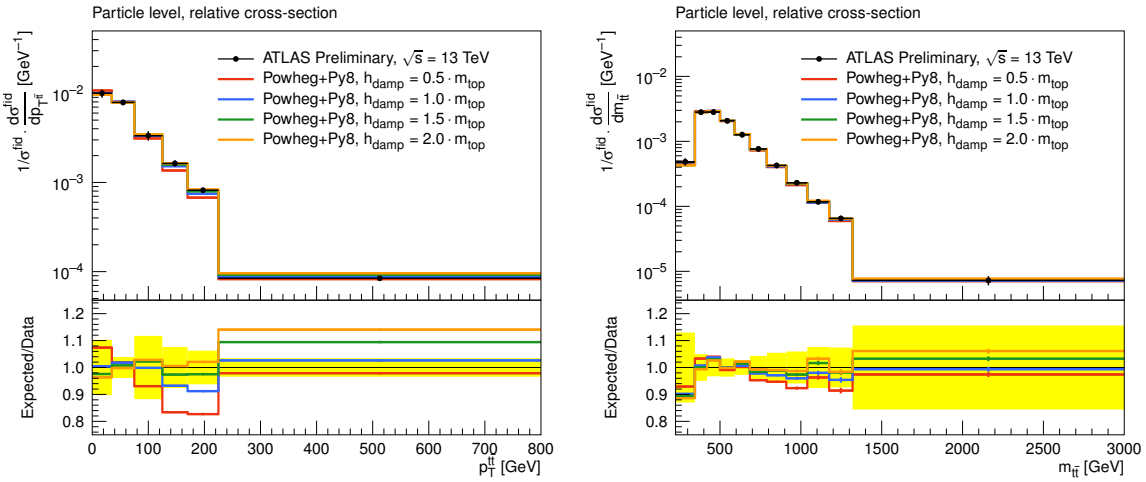

(a) (b)

Figure 3: The Powheg+Pythia8 samples with different h_{damp} variations are compared to data at $\sqrt{s} = 13$ TeV. The comparison is performed for (a) the transverse momentum of the $t\bar{t}$ system and (b) the invariant mass of the $t\bar{t}$ system in $t\bar{t}$ lepton+jets events (resolved channel) using ATLAS data unfolded to particle level in Analysis C [35]. The data and generator predictions are presented the same way as in Fig. 1.

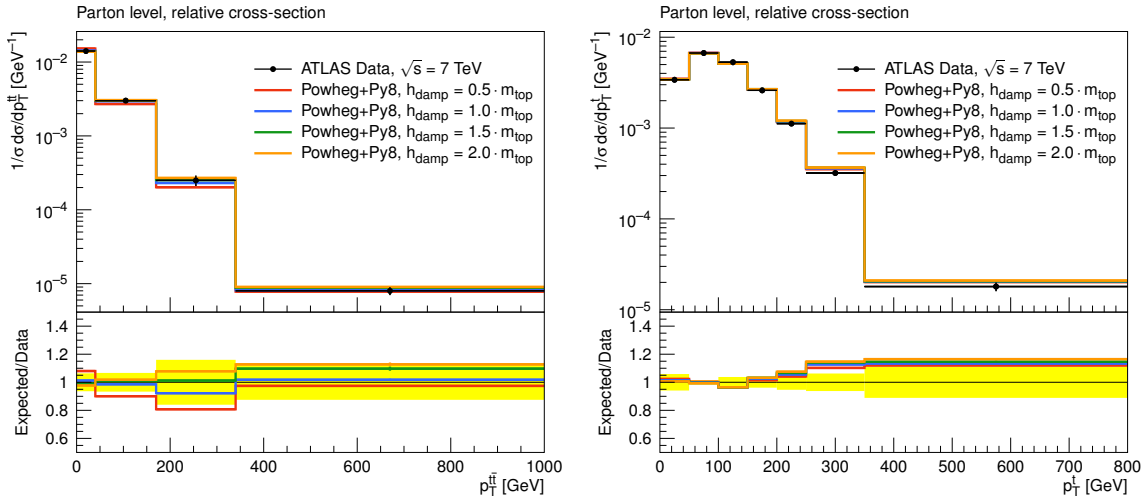

(a) (b)

Figure 4: The POWHEG+PYTHIA8 samples with different h_{damp} variations are compared to data at $\sqrt{s}$ = 7 TeV. The comparison is performed for (a) the transverse momentum of the $t\bar{t}$ system and (b) the transverse momentum of the top quark in $t\bar{t}$ lepton+jets events (resolved channel) using ATLAS data unfolded to parton level in Analysis D [36]. The data and generator predictions are presented the same way as in Fig. 1.

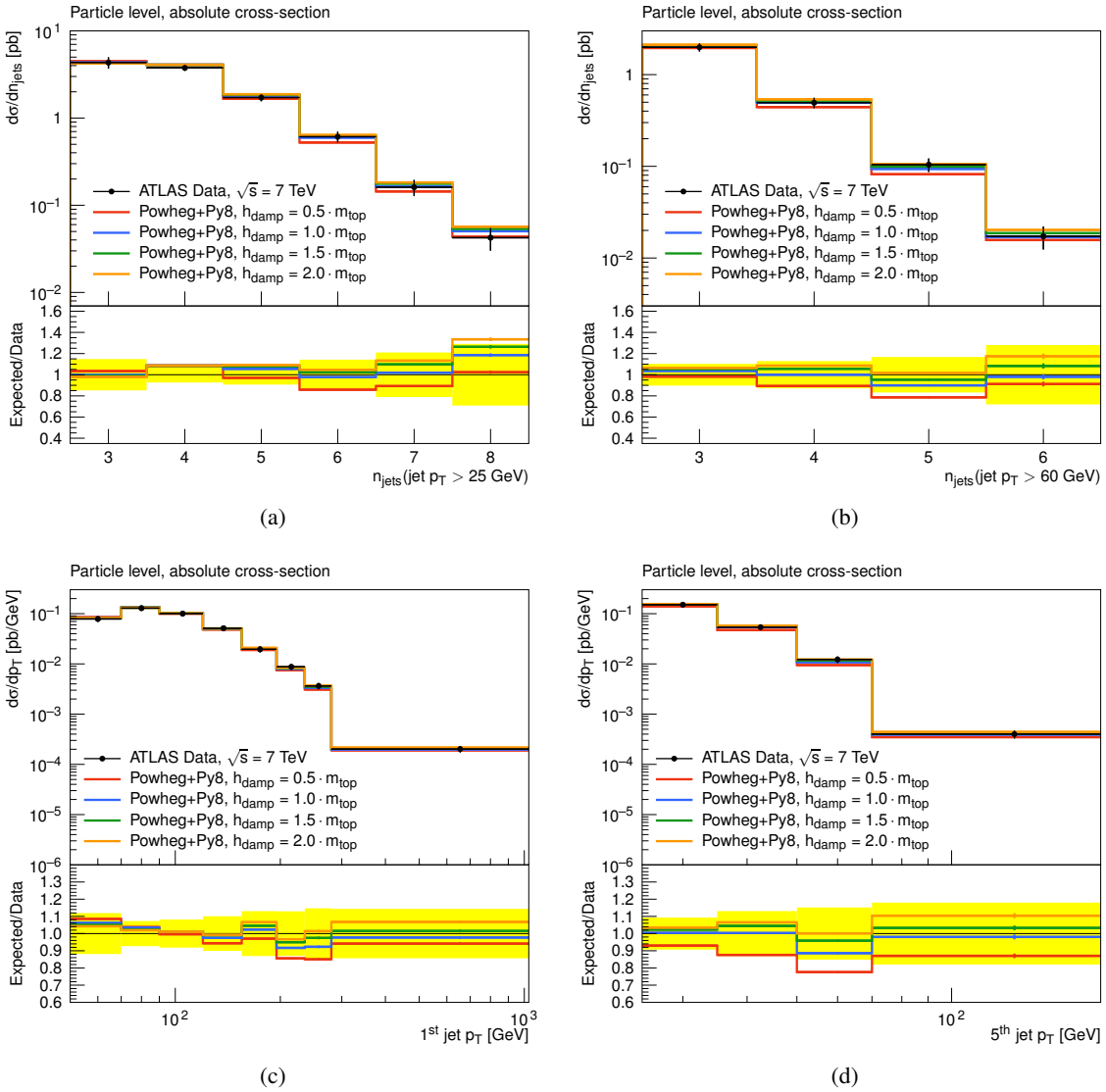

Figure 5: The POWHEG+PYTHIA8 samples with different h_{damp} variations are compared to data at $\sqrt{s} = 7$ TeV. The comparison is performed for the number of jets with (a) $p_{\text{T}} > 25$ GeV and (b) > 60 GeV as well as for the transverse momenta (c) for the leading jet and (d) for the 5th leading jet in $t\bar{t}$ lepton+jets events (resolved channel) using ATLAS data unfolded to particle level in Analysis E [37]. The data and generator predictions are presented the same way as in Fig. 1.

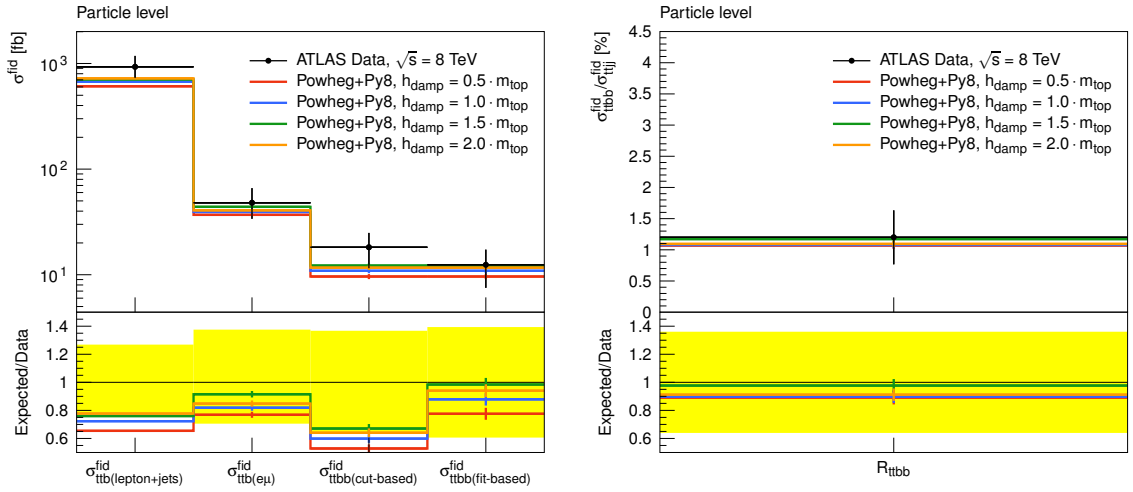

(a) (b)

Figure 6: The POWHEG+PYTHIA8 samples with different h_{damp} variations are compared to data at $\sqrt{s} = 8\,\text{TeV}$. The comparison is performed using ATLAS data unfolded to particle level in Analysis F [38], (a) for the fiducial cross-sections for $t\bar{t}$ production with one or two additional b-jets, and (b) for the ratio of $t\bar{t}$ production with two additional b-jets to $t\bar{t}$ production with any two additional jets. The data and generator predictions are presented the same way as in Fig. 1.

2.2.2 Choice of `main31` p_{T} parameters

Studies of the `main31` p_{T} parameters were initially performed in Ref. [2], where `pTdef` and `pTemt` were varied. The studies on the h_{damp} value setting presented in this note use the POWHEG+PYTHIA8 `main31` parameters which resulted from that initial study. Recent empirical studies with dijet events [39] have shown that `pTdef` and `pThard` are both important parameters ruling the choice of the p_{T} definition for Initial State Radiation (ISR) and Final State Radiation (FSR), and the procedure to calculate the matching scale, respectively, and which should be varied and compared with data to ensure the best overall prediction. The definitions of the parameters which were varied in this study are shown in Table 2 and Table 3. For all samples compared in this section, the h_{damp} value is set to $1.5 \cdot m_{\mathrm{top}}$. For the studies in the previous section, `pTdef` was set to 2 and `pThard` was set to 0. In Fig. 7 one can see that the impact of the `pTdef` and `pThard` variation is quite small. Additional distributions were checked with these parameters but the size of the resulting variations were of the same order as those shown here. As such, the conclusion is that the current default setup with `pTdef` = 2 and `pThard` = 0 provides a good description of the data. Therefore these values will be used for further studies shown in this note.

`pTdef`	Definition
0	POWHEG ISR p_{T} definition is used for both ISR and FSR.
1	POWHEG ISR and FSR p_{T} definitions.
2	PYTHIA ISR and FSR definitions.

Table 2: Summary of the `pTdef` definitions tested in the PYTHIA8 `main31` routine [17, 40].

`pThard`	Definition
0	Q_{fac}.
1	The p_{T} of the POWHEG emission is tested against all other incoming and outgoing partons, with the minimal value chosen.
2	The p_{T} of all final-state partons is tested against all other incoming and outgoing partons, with the minimal value chosen.

Table 3: Summary of the `pThard` definitions tested in the PYTHIA8 `main31` routine to calculate the matching scale [17, 40].

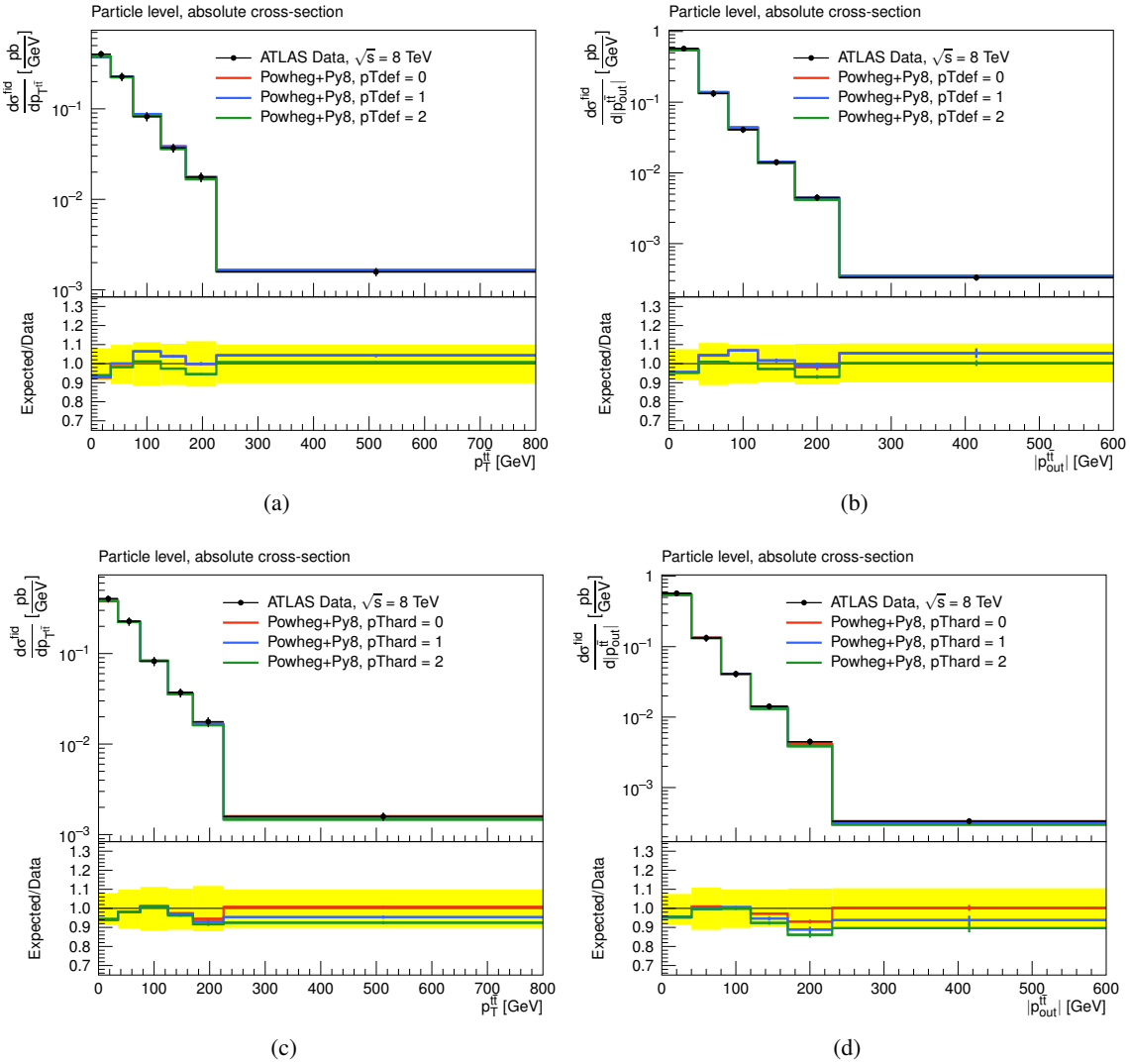

Figure 7: The POWHEG+PYTHIA8 samples with different `pTdef` and `pThard` variations are compared to data at $\sqrt{s} = 8$ TeV. The comparison is performed (a) for the transverse momentum of the $t\bar{t}$ system and (b) for the out-of-plane momentum for different `pTdef` values as well as (c) for the transverse momentum of the $t\bar{t}$ system and (d) for the out-of-plane momentum for different `pThard` values in $t\bar{t}$ lepton+jets events (resolved channel) using ATLAS data unfolded to particle level in Analysis A [29]. The data and generator predictions are presented the same way as in Fig. 1.

2.2.3 POWHEG+PYTHIA8 scale variations

Based on the findings in the previous sections, the best description of the 8 and 13 TeV data for the POWHEG+PYTHIA8 setup is obtained with the h_{damp} parameter set to $1.5 \cdot m_{\text{top}}$, `pTdef` = 2 and `pThard` = 0. To assess the impact of variations of the amount of additional radiation on the distributions under study, two samples are compared to the nominal sample to determine sensible systematic variations based on the parameters just described. The two samples have the following setup:

- The factorisation and renormalisation scales are coherently varied by a factor of 2.0, and the Var3c down variation from the A14 tune is used.
- The factorisation and renormalisation scales are coherently varied by a factor of 0.5, and the Var3c up variation from the A14 tune is used.

The Var3c A14 tune variation [18] corresponds to the varying α_s which impacts ISR in the A14 tune and it was shown in Ref. [2] that this variation covers the size of the other available A14 eigentune variations. Coupled with the relevant scale variations, this results in an estimation of the radiation uncertainty which appears to be slightly conservative. In the distributions shown for the 8 TeV data one can see that the variations partly bracket the nominal prediction and the data, but are a bit smaller than the uncertainties on the data for the low bins of Figs. 8(a)–8(c) and larger than the uncertainties on the data for the high bins. In addition the transverse momentum and the invariant mass of the $t\bar{t}$ system are shown in Fig. 9 for 13 TeV data. In those distributions a similar trend is shown, however the deviation at large transverse $t\bar{t}$ momenta is even larger than for 8 TeV data. Further studies may thus be necessary to find the best setup for the radiation systematic uncertainty.

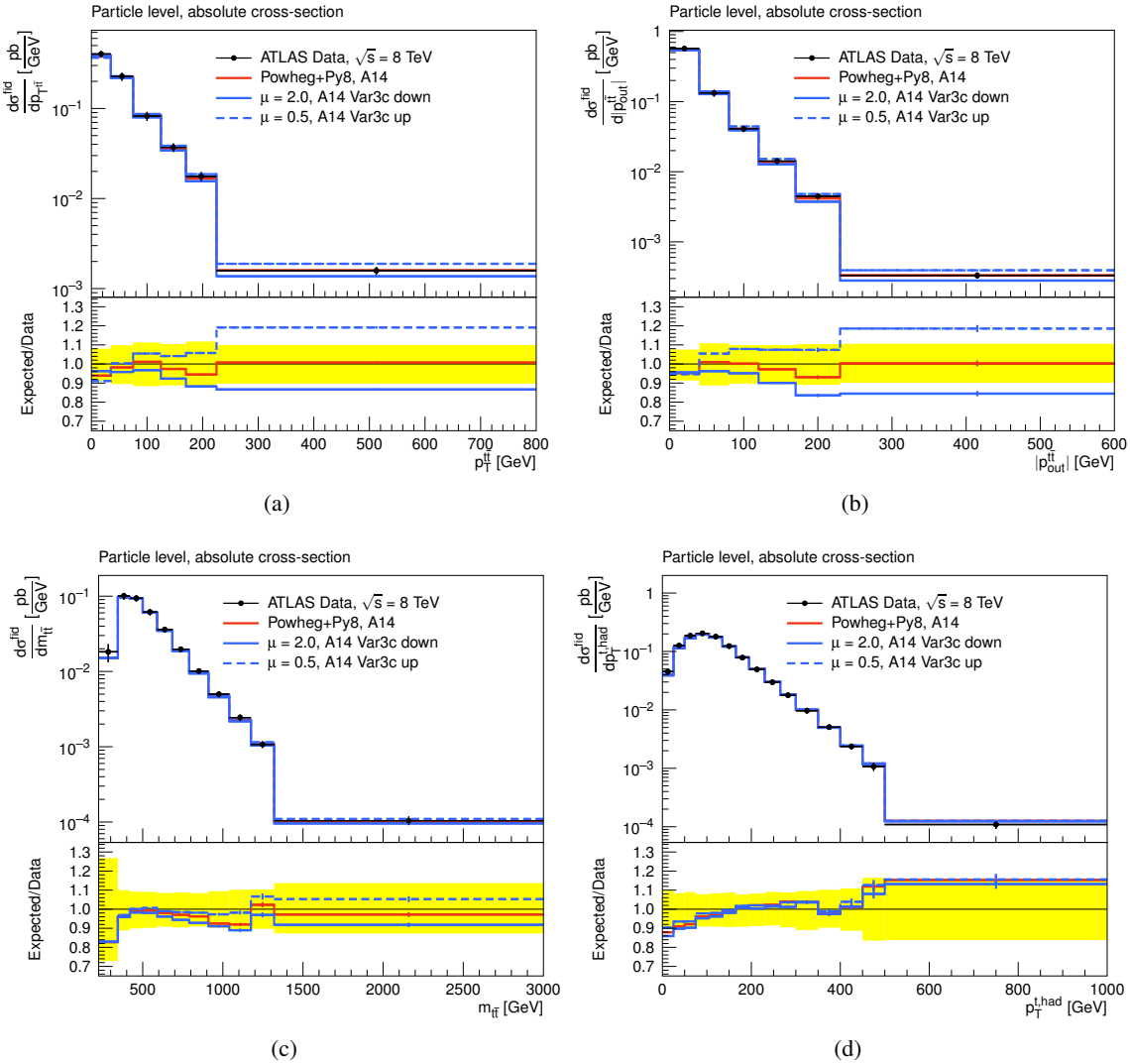

Figure 8: The POWHEG+PYTHIA8 samples with different scale and tune variations are compared to data at $\sqrt{s} = 8$ TeV. The comparison is performed for (a) the transverse momentum of the $t\bar{t}$ system, (b) the out-of-plane momentum, (c) the invariant mass of the $t\bar{t}$ system, and (d) the transverse momentum of the hadronic top quark candidate in $t\bar{t}$ lepton+jets events (resolved channel) using ATLAS data unfolded to particle level in Analysis A [29]. The data and generator predictions are presented the same way as in Fig. 1. The nominal generator prediction is shown as a solid red line, while the scale variation samples are shown in solid and dashed blue lines.

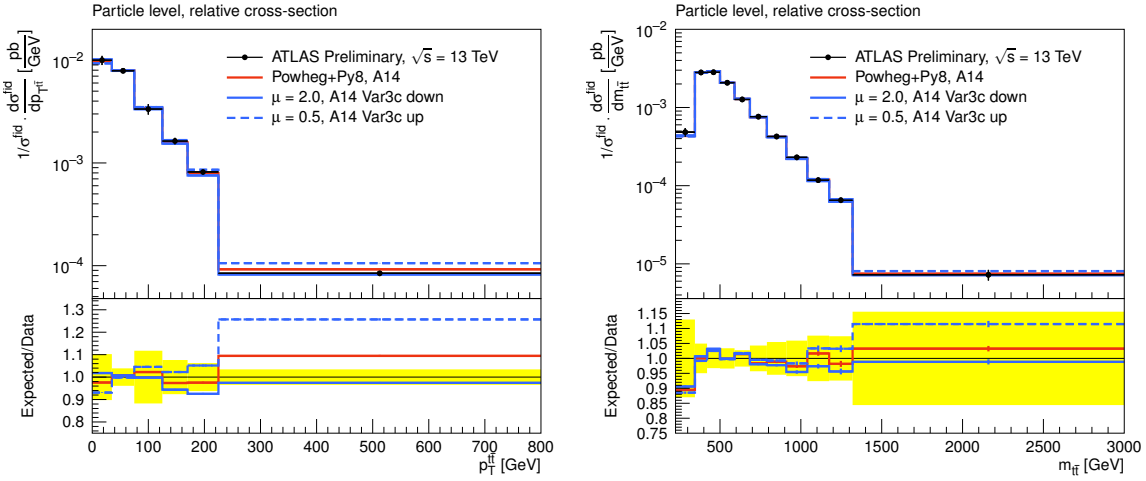

(a) (b)

Figure 9: The POWHEG+PYTHIA8 samples with different scale and tune variations are compared to data at $\sqrt{s} = 13$ TeV. The comparison is performed for (a) the transverse momentum of the $t\bar{t}$ system and (b) the invariant mass of the $t\bar{t}$ system in $t\bar{t}$ lepton+jets events (resolved channel) using ATLAS data unfolded to particle level in Analysis C [35]. The data and generator predictions are presented the same way as in Fig. 1.

2.3 Optimisation studies for POWHEG+HERWIG7

In this section studies of h_{damp} and a parameter concerning the treatment of the global momentum recoils at the end of the showering (`KinematicsReconstructor:ReconstructionOption`) for the HERWIG7 angular-ordered shower are presented. The h_{damp} studies complement the similar studies performed for the POWHEG+PYTHIA8 setup, while the study of the `ReconstructionOption` is used to find the best option among the available ones.

2.3.1 Optimisation of h_{damp}

In order to ensure consistent behaviour of h_{damp} together with PYTHIA8 and HERWIG7, samples with modified values are produced. The most sensitive observable for h_{damp} is the p_{T} of the $t\bar{t}$ system. Fig. 10 shows these distributions for different values of h_{damp} on parton and particle level. It can be seen that on parton level the choices $h_{\text{damp}} = m_{\text{top}}$ and $h_{\text{damp}} = 1.5 \cdot m_{\text{top}}$ are equally good, while on particle level $h_{\text{damp}} = 1.5 \cdot m_{\text{top}}$ is slightly preferred. This is in agreement with the findings for POWHEG+PYTHIA8 and will be used in the following studies.

2.3.2 Study of different kinematic reconstruction options of the HERWIG7 showering

In this section several treatments of the global momentum recoil at the end of the showering for the angular-ordered HERWIG7 shower are presented. With the update from HERWIG++ to HERWIG7, the authors introduced several new methods for shower reconstruction. The momentum reshuffling at the end of the shower is especially important for the modelling of the top-quark p_{T} [11]. The different treatments can be chosen using the parameter `/Herwig/Shower/KinematicsReconstructor:ReconstructionOption`. According to the HERWIG7 manual the allowed values are (explanations taken from the manual): C

- `General` Use the general solution which ignores the colour structure for all processes.
- `Colour` Use the colour structure of the process to determine the reconstruction procedure. This option is called “Colour1” in the following studies.
- `Colour2` Make the most use possible of the colour structure of the process to determine the reconstruction procedure. Start with final–final-state, then inital–final-state then inital–inital-state colour connections.
- `Colour3` Make the most use possible of the colour structure of the process to determine the reconstruction procedure. Do the colour connections in order of the p_{T}’s emitted in the shower starting with the hardest. The colour partner is fully reconstructed at the same time.
- `Colour4` Make the most use possible of the colour structure of the process to determine the reconstruction procedure. Do the colour connections in order of the p_{T}’s emitted in the shower starting with the hardest, while leaving the colour partner on mass-shell.

The recommended value from the HERWIG7 authors is `Colour3`. Most sensitive observables for these settings are again distributions connected with the $t\bar{t}$ system, but also distributions from the top quark itself. Figure 11 shows distributions of the $t\bar{t}$ system on parton and particle level. The distribution of the p_{T} $(t\bar{t})$ is modelled very well by samples using options `Colour3` or `Colour4`, while all other options produce distributions close or outside of the experimental uncertainty band. The $m(t\bar{t})$ distribution has the

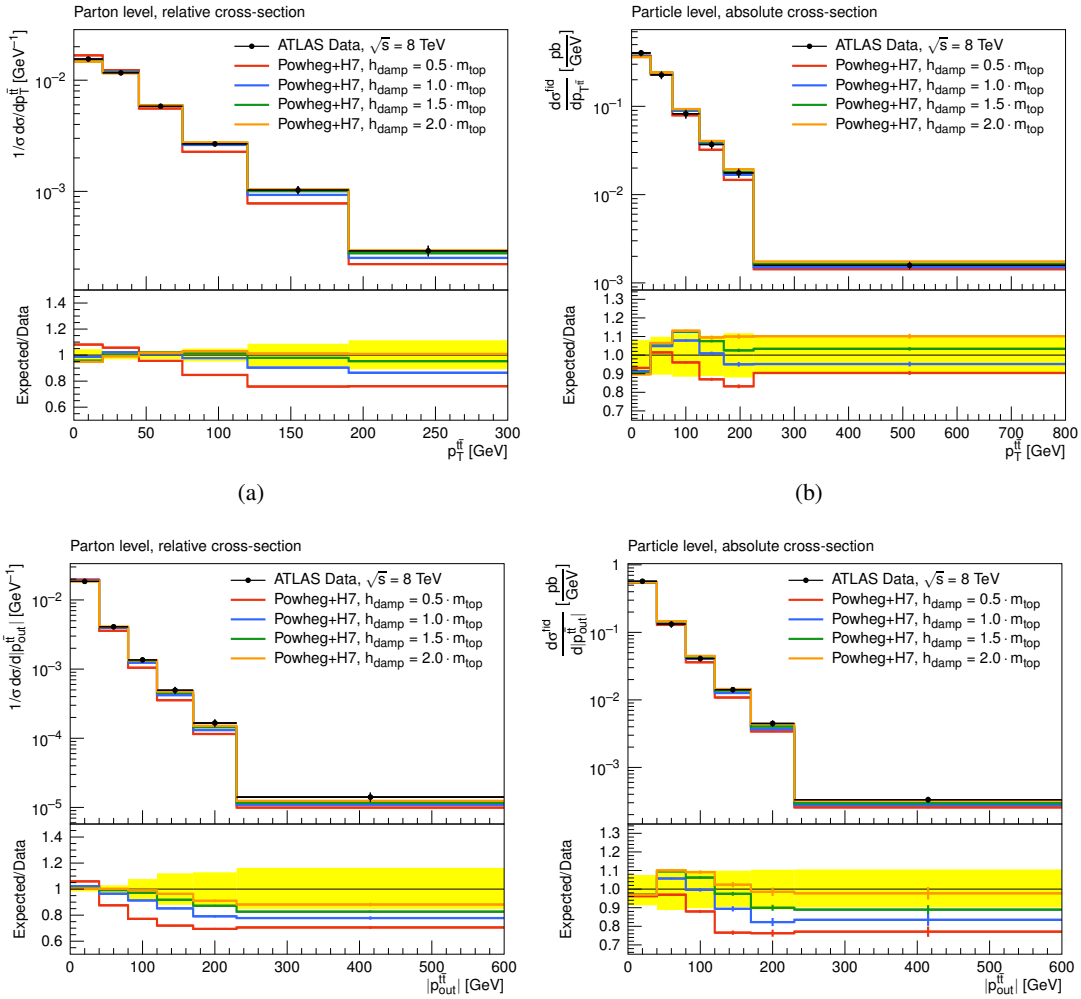

Figure 10: The POWHEG+HERWIG7 samples with different h_{damp} values are compared to data at $\sqrt{s} = 8$ TeV. The comparison is performed for (a) and (b) the p_{T} of the $t\bar{t}$ system, (c) and (d) the out-of-plane p_{T} of the $t\bar{t}$ system from Analysis A [29] in $t\bar{t}$ lepton+jets events using ATLAS data unfolded to (left) parton level and (right) particle level. The data and generator predictions are presented the same way as in Fig. 1.

best modelling for `Colour2`, but with this setting the distribution of the production angle $\chi(t\bar{t})$, defined as $\chi(t\bar{t}) = e^{2|\Delta y|}$ [41], is outside of the experimental uncertainty band. The same holds for `Colour4`. Distributions of the partonic top quark and the reconstructed top quark are presented in Fig. 12. It can be noted, that the p_{T} of the top quark is almost perfectly modelled using `Colour3` or `Colour4`.
In summary the recommended option `Colour3` has the best performance for all considered distributions.

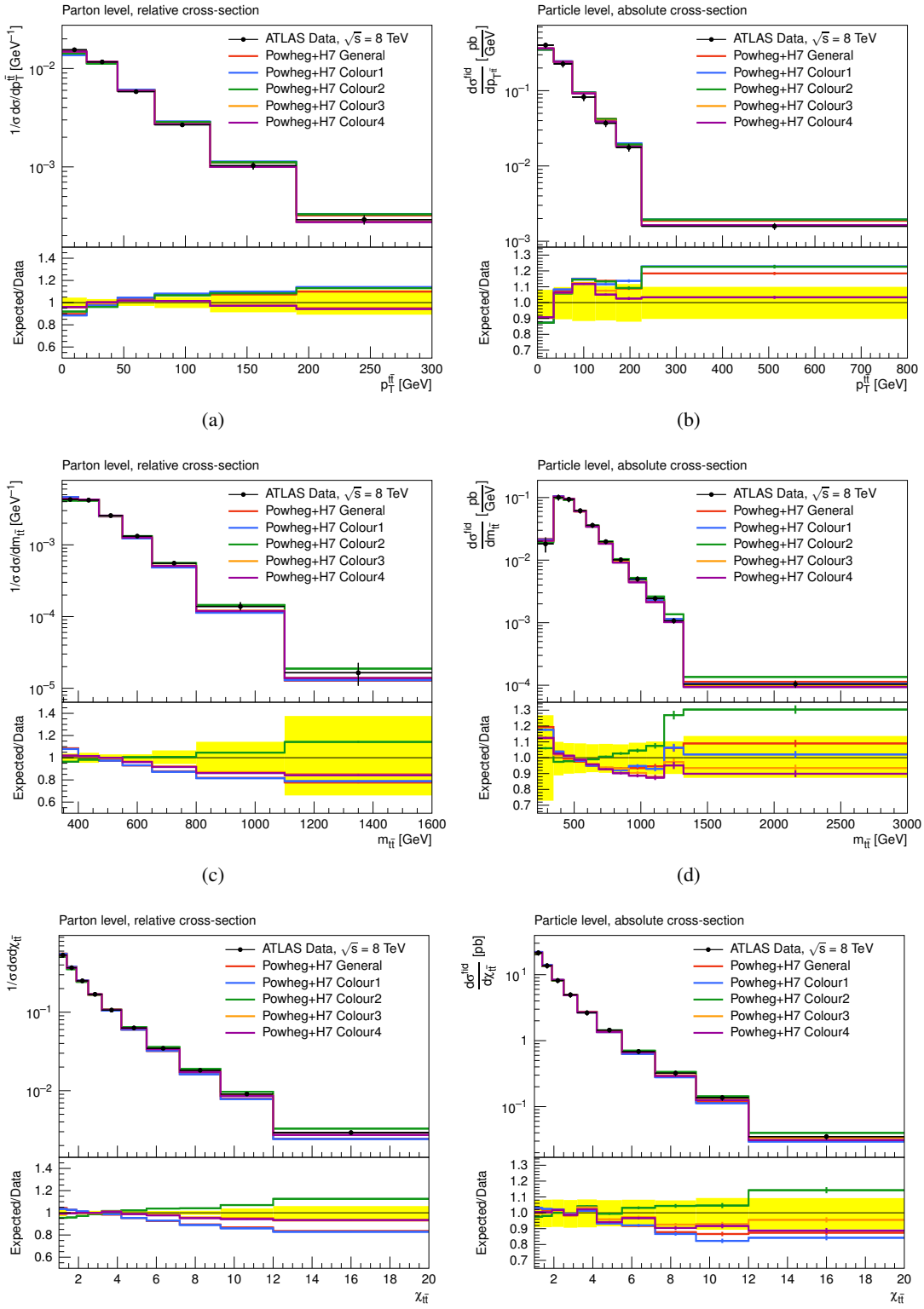

Figure 11: The POWHEG+HERWIG7 samples with different reconstruction options for the shower compared to data at $\sqrt{s} = 8$ TeV. The comparison is performed for (a) and (b) the p_{T} of the $t\bar{t}$ system, (c) and (d) the invariant mass of the $t\bar{t}$ system, (e) and (f) the $\chi(t\bar{t})$ from Analysis A [29] in $t\bar{t}$ lepton+jets events using ATLAS data unfolded to (left) parton level and (right) particle level. The h_{damp} value in these studies is set to $1.5 \cdot m_{\mathrm{top}}$. The data and generator predictions are presented the same way as in Fig. 1.

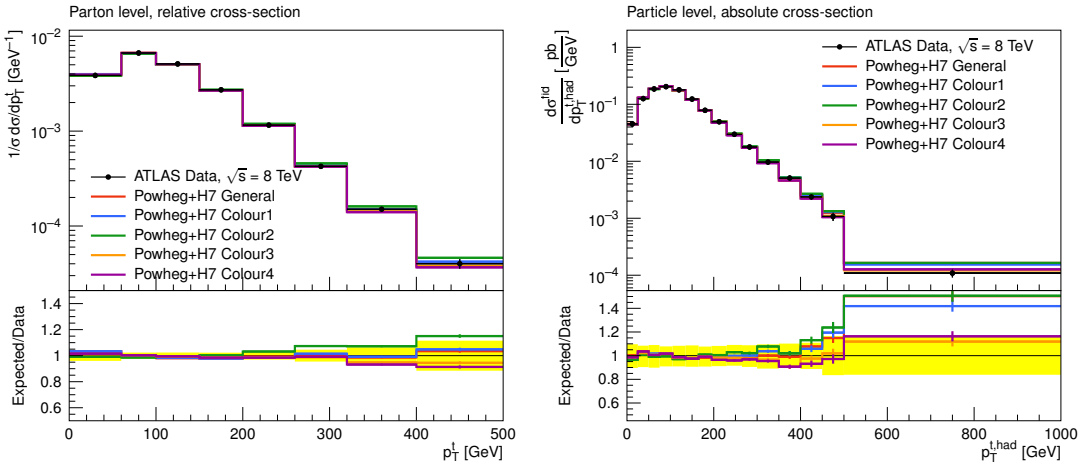

(a) (b)

Figure 12: The POWHEG+HERWIG7 samples with different reconstruction options for the shower compared to data at $\sqrt{s} = 8\,\text{TeV}$. The comparison is performed for (a) and (b) the p_{T} of the $t\bar{t}$ system from Analysis A [29] in $t\bar{t}$ lepton+jets events using ATLAS data unfolded to (left) parton level and (right) particle level. In most of the cases the purple and the orange lines do overlap perfectly, such that they can't be seen. The h_{damp} value in these studies is set to $1.5 \cdot m_{\text{top}}$. The data and generator predictions are presented the same way as in Fig. 1.

2.4 Comparison of generator setups

Different generator and parton shower combinations are presented in this section and compared to unfolded $\sqrt{s} = 7, 8$ and 13 TeV data to assess the performance of the $t\bar{t}$ predictions.

2.4.1 Comparison of different parton shower algorithms interfaced to POWHEG

In Fig. 13 different samples generated with POWHEG and interfaced to different parton shower and hadronisation algorithms are compared to 8 TeV data (Analysis A). Differences can be observed in the description of the transverse momentum and the out-of-plane momentum of the $t\bar{t}$ system between POWHEG+PYTHIA8 and POWHEG+HERWIG7 samples in Figs. 13(a) and 13(b). The differences between the samples are of the same order as the uncertainty on the measurement. Similar differences are observed for the transverse momentum of the $t\bar{t}$ system in Fig. 15(a) for 13 TeV data (Analysis C).

The transverse momentum of the top-jet in the boosted regime can be seen in Fig. 14 (Analysis B), where the three different POWHEG samples are compared. The description of high p_{T} data is better with PYTHIA8 compared to either PYTHIA6 or HERWIG7.

For the measurement of the the top-quark p_{T} at 13 TeV shown in Fig. 15(c), the best agreement is achieved with POWHEG+HERWIG7, similar to the agreement seen with 8 TeV data shown in Fig. 13(d). However, when considering the $t\bar{t}$ invariant mass, POWHEG interfaced to PYTHIA6 or PYTHIA8 provides a much better description of the data than POWHEG+HERWIG7, both at 8 TeV (Fig. 13(c)) and at 13 TeV (Fig. 15(b)).

The distributions with $\sqrt{s} = 7$ TeV data (Analysis E) in Fig. 16 clearly shows a feature of the current HERWIG7 setup described in [3], namely increased jet activity which is not in agreement with the PYTHIA parton showers or with the data. Due to the higher jet activity the amount of heavy flavour production is over-predicts in HERWIG7, as shown in Fig. 17 (Analysis F). There is good agreement between the POWHEG samples interfaced to PYTHIA6 and PYTHIA8 and with data in Fig. 16 and 17. The description of the number of high-p_{T} jets in data is also good with POWHEG+PYTHIA8.

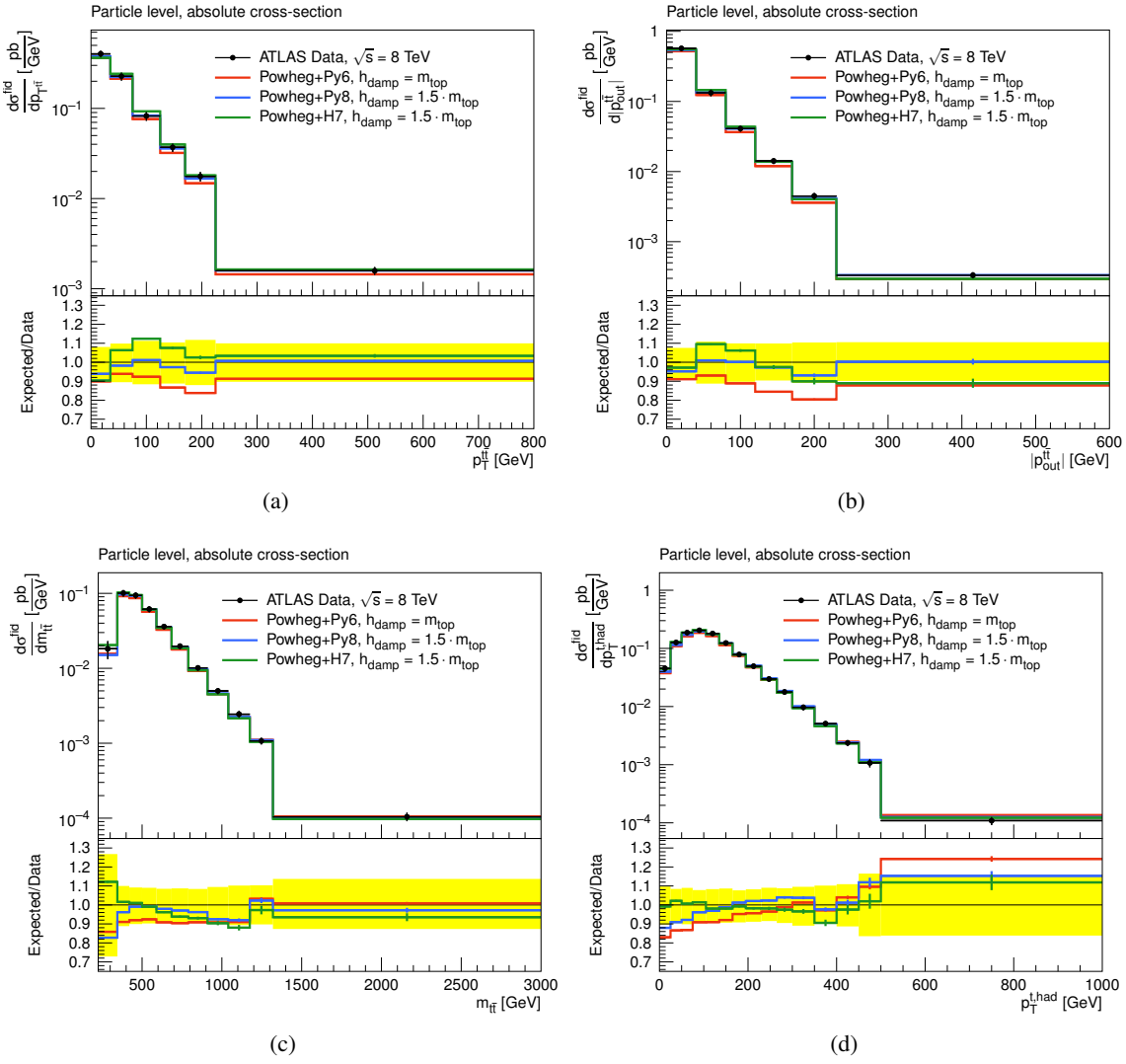

Figure 13: The POWHEG samples with different parton shower and hadronisation algorithms are compared to data at $\sqrt{s}$ = 8 TeV. The comparison is performed (a) for the transverse momentum of the $t\bar{t}$ system, (b) for the out-of-plane momentum, (c) for the invariant mass of the $t\bar{t}$ system, and (d) for the transverse momentum of the hadronic top quark candidate in $t\bar{t}$ lepton+jets events (resolved channel) using ATLAS data unfolded to particle level in Analysis A [29]. The data and generator predictions are presented the same way as in Fig. 1.

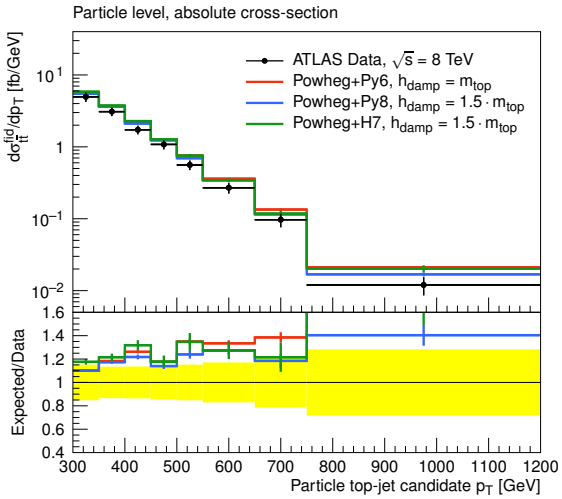

Figure 14: The POWHEG samples with different parton shower and hadronisation algorithms are compared to data at $\sqrt{s} = 8$ TeV. The comparison is performed for the particle top-jet p_{T} candidate using ATLAS data unfolded to particle level in Analysis B [34]. The data and generator predictions are presented the same way as in Fig. 1.

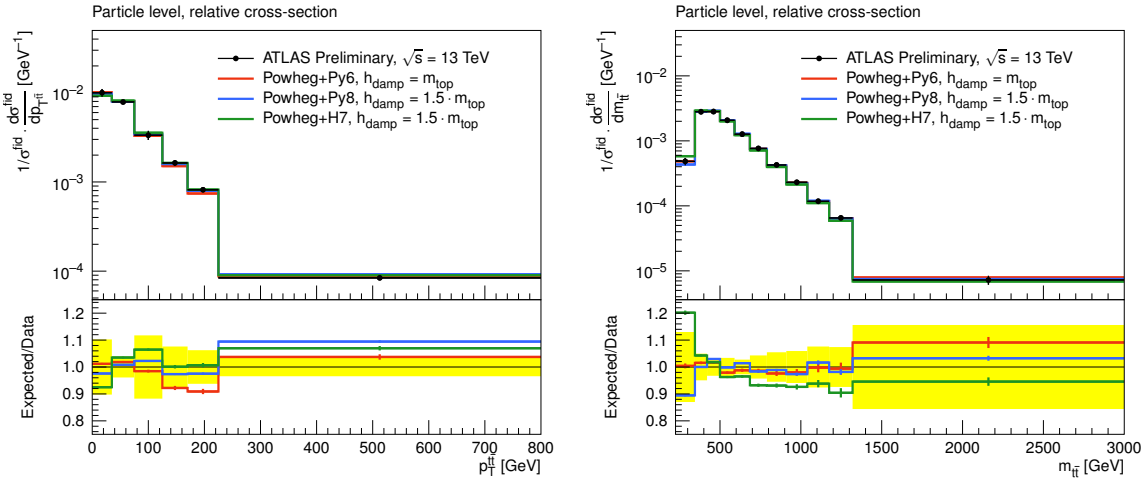

(a) (b)

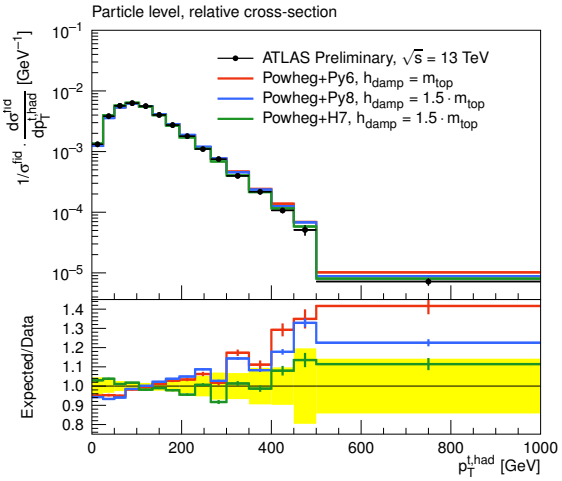

(c)

Figure 15: The POWHEG samples with different parton shower and hadronisation algorithms are compared to data at $\sqrt{s} = 13$ TeV. The comparison is performed (a) for the transverse momentum of the $t\bar{t}$ system, (b) for the invariant mass of the $t\bar{t}$ system, and (c) for the transverse momentum of the hadronic top-quark candidate in $t\bar{t}$ lepton+jets events (resolved channel) using ATLAS data unfolded to particle level in Analysis C [35]. The data and generator predictions are presented the same way as in Fig. 1.

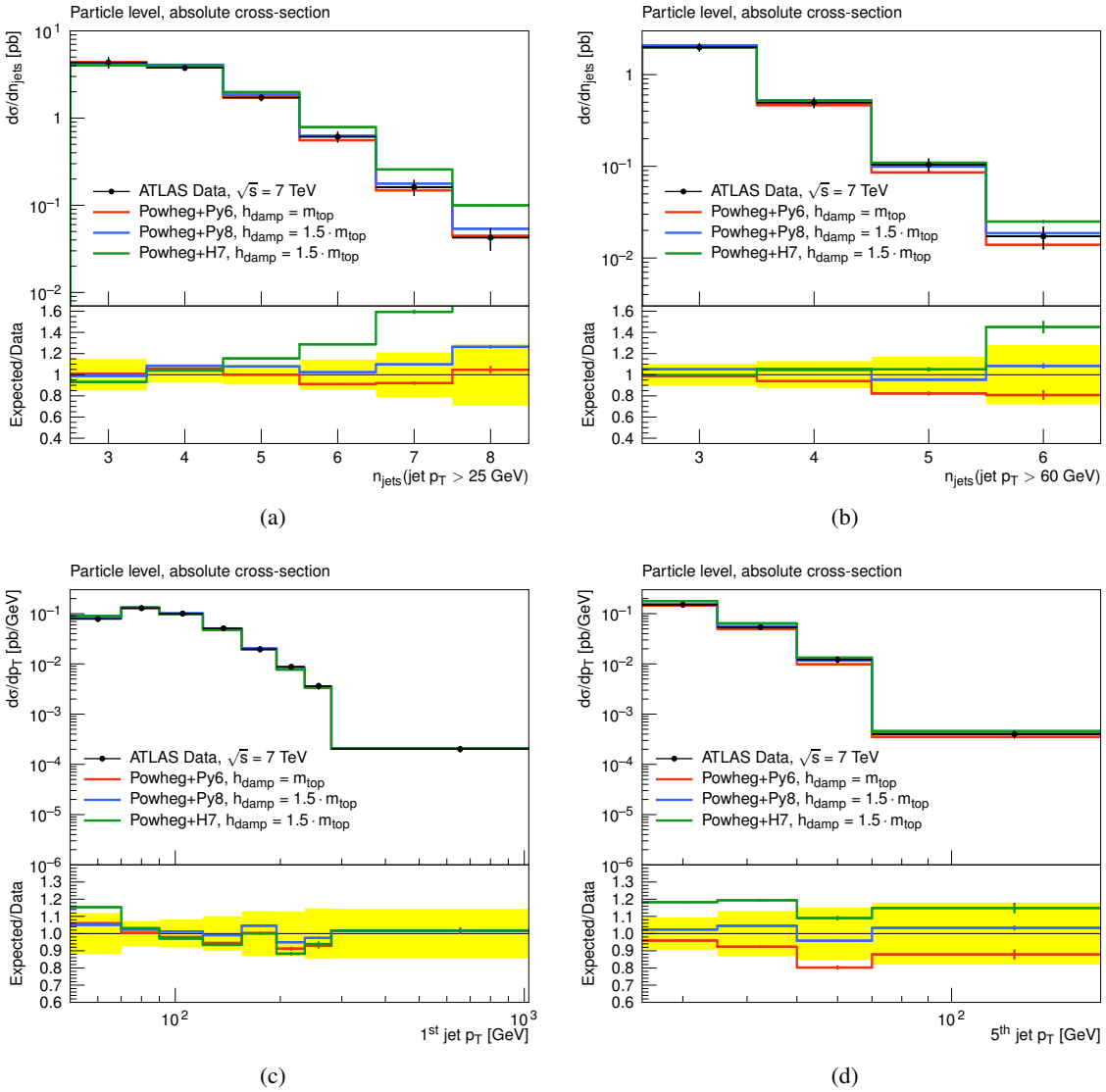

Figure 16: The POWHEG samples with different parton shower and hadronisation algorithms are compared to data at $\sqrt{s}$ = 7 TeV. The comparison is performed for the number of jets with (a) $p_{\mathrm{T}} > 25$ GeV and (b) > 60 GeV as well as for the transverse momenta (c) for the leading jet and (d) for the 5th leading jet in $t\bar{t}$ lepton+jets events (resolved channel) using ATLAS data unfolded to particle level in Analysis E [37]. The data and generator predictions are presented the same way as in Fig. 1.

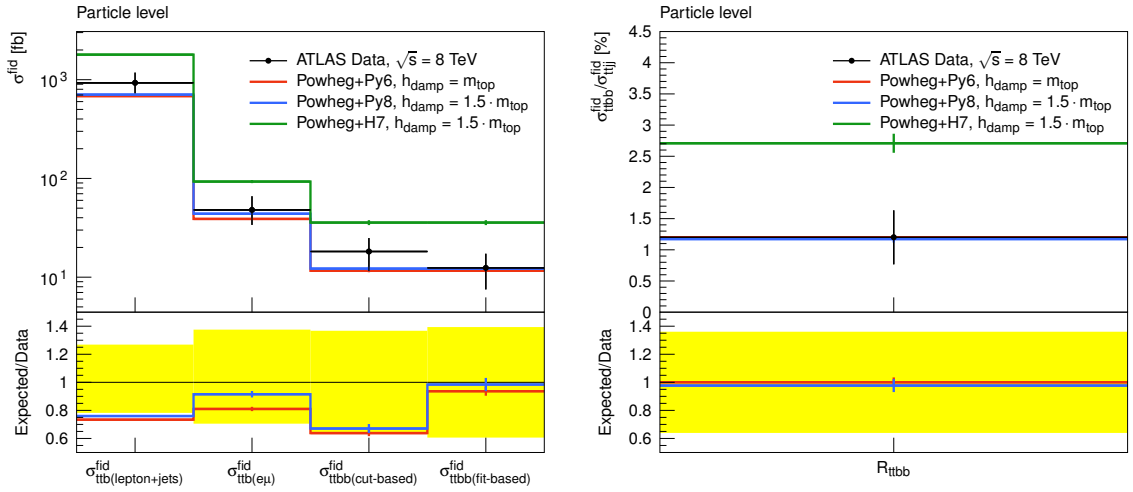

(a) (b)

Figure 17: The POWHEG samples with different parton shower and hadronisation algorithms are compared to data at $\sqrt{s} = 8$ TeV. The comparison is performed using ATLAS data unfolded to particle level in Analysis F [38], (a) for the fiducial cross-sections for $t\bar{t}$ production with one or two additional b-jets, and (b) for the ratio of $t\bar{t}$ production with two additional b-jets to $t\bar{t}$ production with any two additional jets. The data and generator predictions are presented the same way as in Fig. 1.

2.4.2 Comparison of matrix-element generators

In Figs. 18–22, the optimal Powheg+Pythia8 setup resulting from the studies presented in this note is compared with MG5_aMC@NLO+Pythia8 which models $t\bar{t}$ inclusively at NLO precision, with MG5_aMC@NLO+Pythia8 which uses the FxFx merging prescription to describe up to two additional partons at NLO accuracy, and with Sherpa 2.2 which uses MEPS@NLO merging to describe up to one additional parton at NLO accuracy and up to four additional partons at LO accuracy.

In Fig. 18 results are compared to the $\sqrt{s} = 8\,\text{TeV}$ data using Analysis A. The two multi-leg generators MG5_aMC@NLO+Pythia8 + FxFx and Sherpa 2.2 perform equally well in all four investigated observables. Differences are present for MG5_aMC@NLO+Pythia8 in case of $p_{\text{T}}(t\bar{t})$ and for Powheg+Pythia8 in case of $m(t\bar{t})$. For the latter the differences are within the uncertainties of the measurement. The different shape of the $m(t\bar{t})$ distinguishes between different NLO subtraction methods. It can also be noted, that the $|p^{t\bar{t}}_{\text{out}}|$ distribution of MG5_aMC@NLO+Pythia8 indicates that the amount of additional radiation is not well modelled. These conclusion are confirmed by comparisons with $\sqrt{s} = 13\,\text{TeV}$ data recorded in Analysis C as shown in Fig. 20. The modelling of the top-quark p_{T} is of special interest, since several analyses found discrepencies between the measurement and predictions of the MC generators. While the distribution agrees well within the uncertainty of the measurement in $\sqrt{s} = 8\,\text{TeV}$, there is a clear slope observed in the distributions at $\sqrt{s} = 13\,\text{TeV}$ using measurements from Analysis C. The p_{T} distribution measured at $\sqrt{s} = 8\,\text{TeV}$ in a boosted regime using Analysis B, see Fig. 19, is not sensitive enough.

Apart from properties of the top quark and the $t\bar{t}$ system, the number of jets and p_{T} of the jets is important. These distributions are shown in Fig. 21 compared to results obtained with $\sqrt{s} = 7\,\text{TeV}$ data of Analysis E.

For the number of jets and the p_{T} of the first and fifth jet, good agreement between data and MC is given by MG5_aMC@NLO+Pythia8 + FxFx, Sherpa 2.2 and Powheg+Pythia8. Sherpa 2.2 predicts too many jets for very high numbers of jets, while MG5_aMC@NLO+Pythia8 under-predicts them. However the predictions of the number of jets, which the generators model at least with LO accuracy, are all within the uncertainties of the measurements. For the leading jet p_{T}, MG5_aMC@NLO+Pythia8 gives a softer spectrum than observed in data.

Finally, fiducial cross sections of $t\bar{t}$ production with additional heavy flavour production are compared using $\sqrt{s} = 8\,\text{TeV}$ data from Analysis F in Fig. 22. Since Sherpa 2.2 includes matrix elements with b quarks the predicted fiducial cross sections are higher than those from the other generators, which all give lower predictions than the measured value, but with differences smaller than the uncertainties.

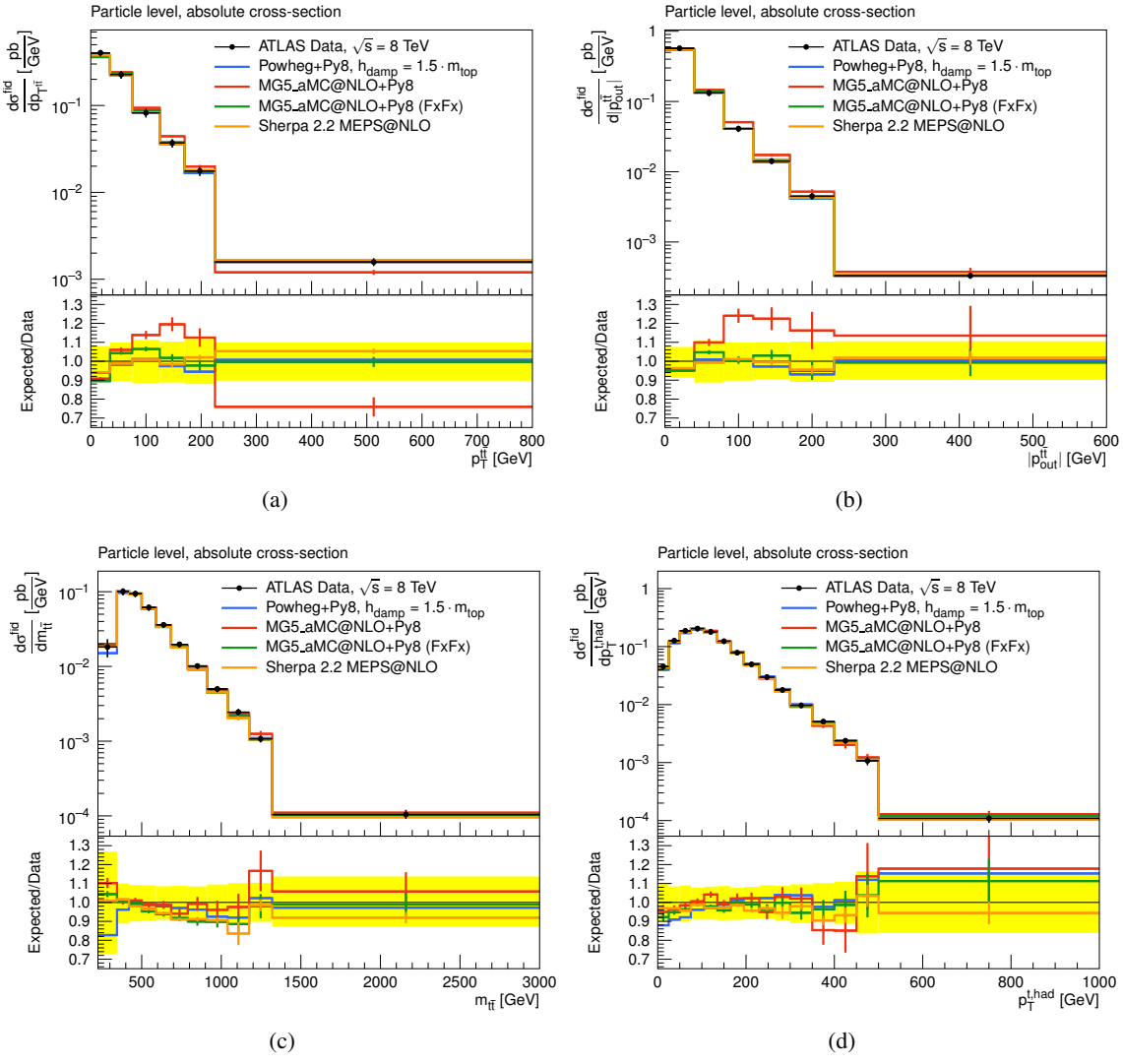

Figure 18: Samples with different generator setups are compared to data at $\sqrt{s} = 8$ TeV. The comparison is performed (a) for the transverse momentum of the $t\bar{t}$ system, (b) the out-of-plane momentum, (c) for the invariant mass of the $t\bar{t}$ system, and (d) for the transverse momentum of the hadronic top quark candidate in $t\bar{t}$ lepton+jets events (resolved channel) using ATLAS data unfolded to particle level in Analysis A [29]. The data and generator predictions are presented the same way as in Fig. 1.

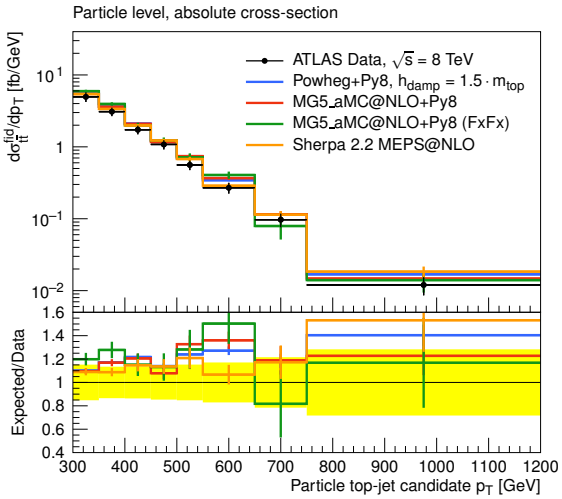

Figure 19: Samples with different generator setups are compared to data at $\sqrt{s} = 8$ TeV. The comparison is performed for the particle top-jet p_{T} candidate using ATLAS data unfolded to particle level in Analysis B [34]. The data and generator predictions are presented the same way as in Fig. 1.

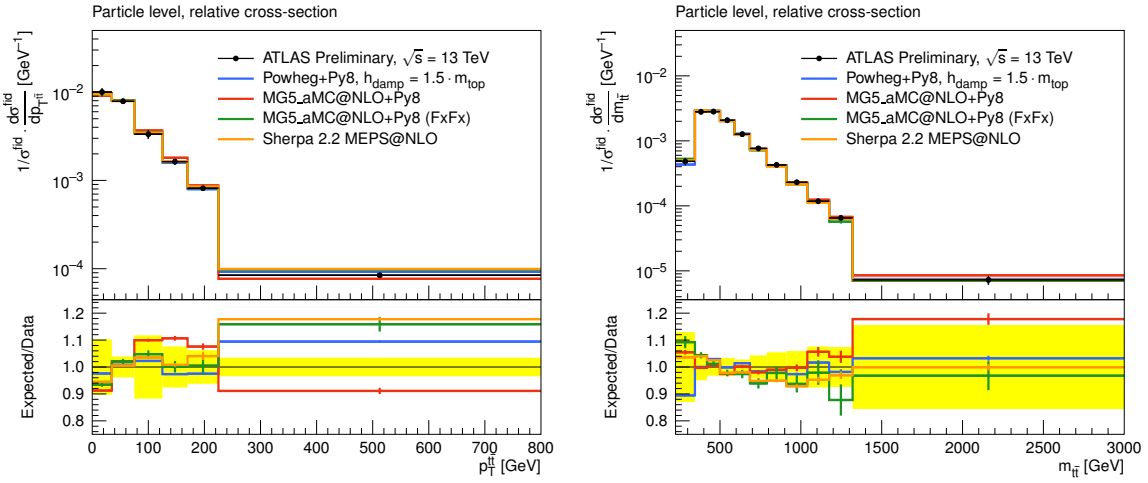

(a) (b)

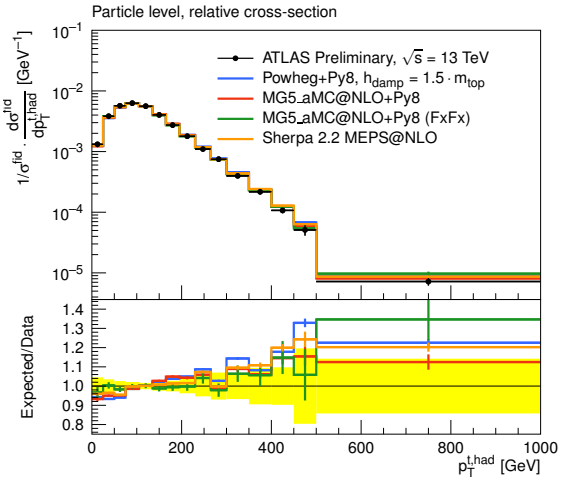

(c)

Figure 20: Samples with different generator setups are compared to data at $\sqrt{s}$ =13 TeV. The comparison is performed (a) for the transverse momentum of the $t\bar{t}$ system, (b) for the invariant mass of the $t\bar{t}$ system, and (c) for the transverse momentum of the hadronic top-quark candidate in $t\bar{t}$ lepton+jets events (resolved channel) using ATLAS data unfolded to particle level in Analysis C [35]. The data and generator predictions are presented the same way as in Fig. 1.

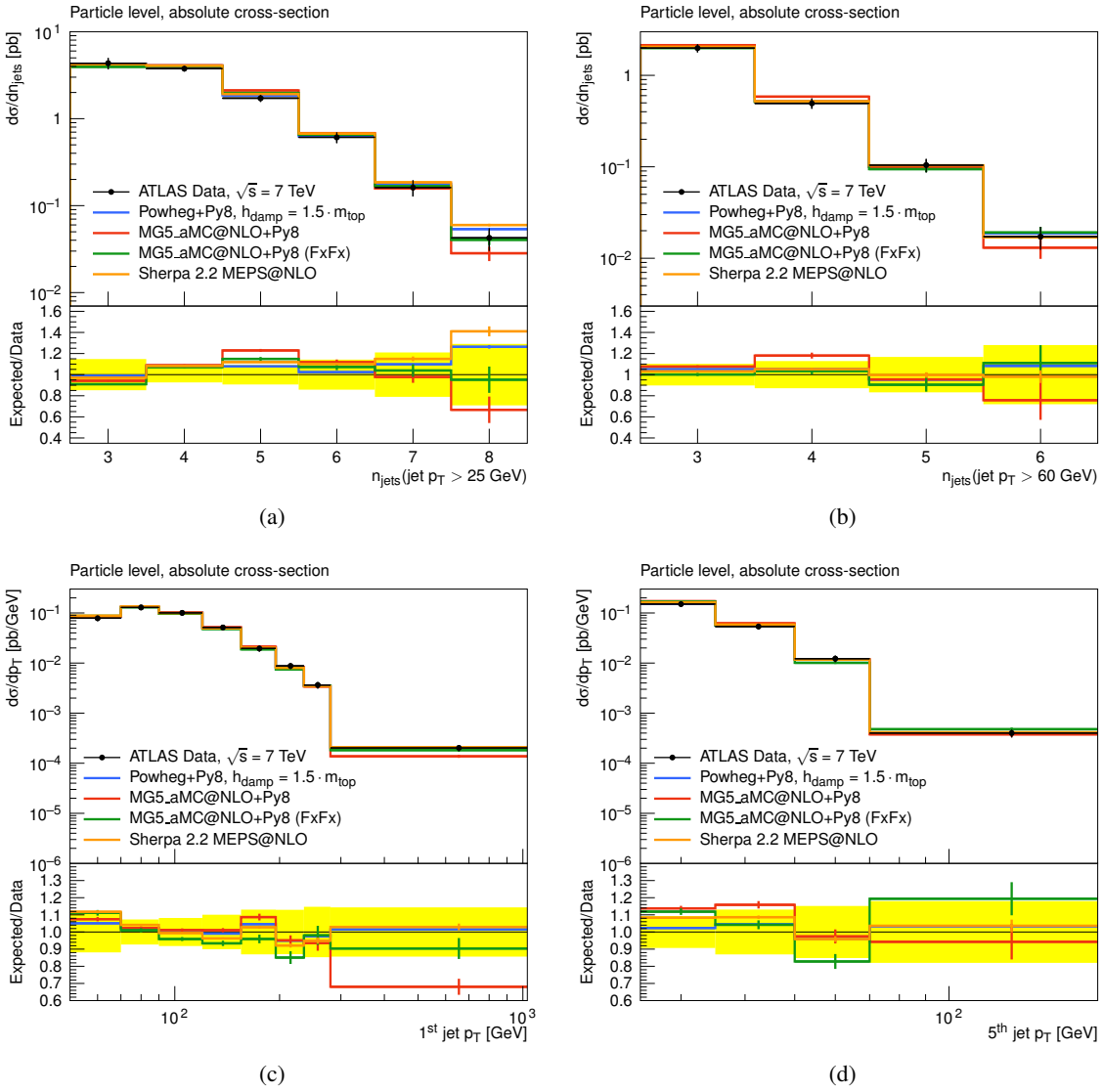

Figure 21: Samples with different generator setups are compared to data at $\sqrt{s}$ =7 TeV. The comparison is performed for the number of jets with (a) $p_{\mathrm{T}} > 25$ GeV and (b) > 60 GeV as well as for the transverse momenta (c) for the leading jet and (d) for the 5th leading jet in $t\bar{t}$ lepton+jets events (resolved channel) using ATLAS data unfolded to particle level in Analysis E [37]. The data and generator predictions are presented the same way as in Fig. 1.

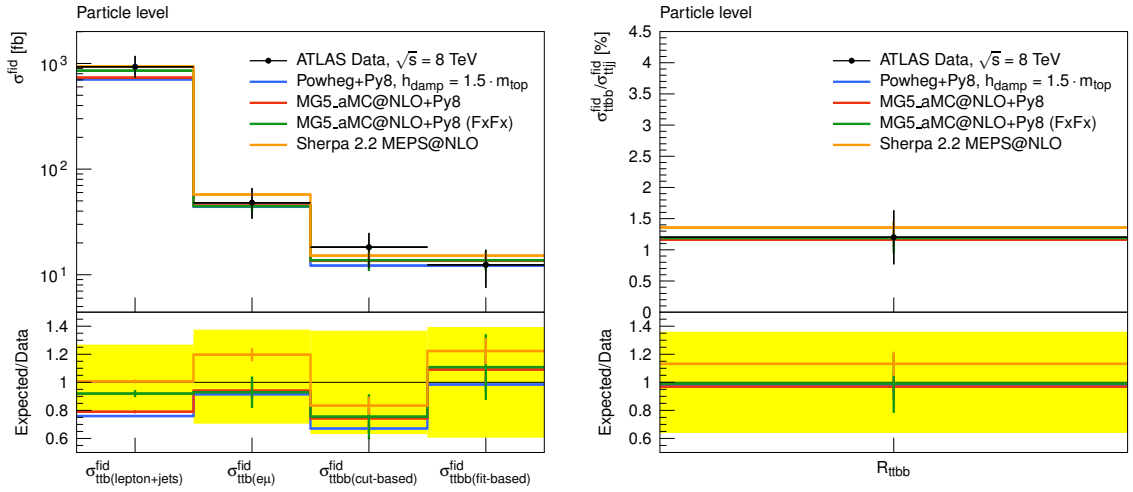

(a) (b)

Figure 22: The POWHEG samples with different parton shower and hadronisation algorithms are compared to data at $\sqrt{s} = 8$ TeV. The comparison is performed using ATLAS data unfolded to particle level in Analysis F [38], (a) for the fiducial cross-sections for $t\bar{t}$ production with one or two additional b-jets, and (b) for the ratio of $t\bar{t}$ production with two additional b-jets to $t\bar{t}$ production with any two additional jets. The data and generator predictions are presented the same way as in Fig. 1.

3 Interference studies of Wt and tWZ processes

At NLO, generating Wt results in the generation of diagrams that overlap with $t\bar{t}$, as illustrated in Fig. 23. Several different methods exist in order to separate between the processes and to remove the overlap to avoid double counting.

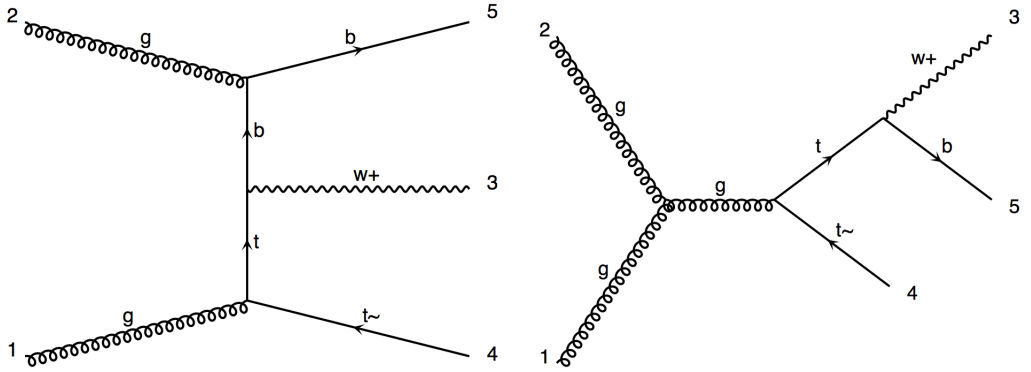

Figure 23: Diagrams generated [21] for Wt production at NLO in the five flavour scheme. A singly-resonant diagram is shown to the left and a doubly-resonant diagram, which overlaps with $t\bar{t}$ production at LO, is shown to the right.

The diagrams that give rise to the overlap contain two top quarks, both of which can be on shell, and are henceforth referred to as doubly-resonant (dr). The diagrams with only one on-shell top quark are called singly-resonant (sr). In equation (2), the amplitude for Wt production is expressed in terms of sr and dr contributions, with the square of this equation giving Eq. (3):

$$\mathcal{M}_{\text{tot}} = \mathcal{M}_{\text{sr}} + \mathcal{M}_{\text{dr}}\,, \tag{2}$$

$$|\mathcal{M}_{\text{tot}}|^2 = |\mathcal{M}_{\text{sr}}|^2 + 2\text{Re}(\mathcal{M}_{\text{sr}} \cdot \mathcal{M}_{\text{dr}}^*) + |\mathcal{M}_{\text{dr}}|^2. \tag{3}$$

In what is commonly known as Diagram Removal (DR), here referred to as Diagram Removal 1, the amplitudes of dr diagrams are set to zero, $\mathcal{M}_{\text{dr}} = 0$. This removes the $t\bar{t}$ contribution as well as the interference between $t\bar{t}$ and Wt - only the first term in Eq. (3) is kept. If the interference is to be neglected, this should be justified by checking its effect in the signal region for the measurement in question. For this a different method needs to be implemented. A procedure that removes the overlap, while also assessing the interference, is the Diagram Subtraction (DS) method [42, 43]. This method, however, relies on momentum reshuffling that introduces uncertainties and dependence on unphysical parameters. The method that is highlighted in this section is referred to as Diagram Removal 2, here implemented in MG5_aMC@NLO, as recently suggested in Ref. [44]. In this method, the amplitude squared of the doubly-resonant diagrams is subtracted from the amplitude squared of the total, thus keeping both the singly-resonant diagrams and the interference of Wt with $t\bar{t}$, while removing the last term in Eq. (3).

When computing the cross section that includes doubly-resonant diagrams for the DR2 procedure, a divergence appears in the top-quark propagator when the top quark is on-shell, shown in the left hand side of Eq. (4). By default, the propagator expression is evaluated with the top quark width Γ_t set to zero in MG5_aMC@NLO. To regularise the integral over the four-momentum, the top-quark width is redefined to the value found in the parameter card, thereby modifying the propagator as

$$\frac{1}{(p_b + p_W)^2 - m_t^2} \rightarrow \frac{1}{(p_b + p_W)^2 - m_t^2 + i m_t \Gamma_t}. \tag{4}$$

Overlapping diagrams also appear for the associated production with a Z or Higgs boson (tWZ, tWH). Diagram Removal 2 can be applied in a similar manner to remove the overlap, while including the interference with $t\bar{t}$, $t\bar{t}Z$ and $t\bar{t}H$. In the case of tWZ, overlaps with $t\bar{t}$ are produced in the channel $t \rightarrow WbZ$, as shown in Fig. 24. The procedure for removing these overlaps is the same as described above, with the addition that for certain diagrams, where a top quark emits a Z boson before decaying, both top-quark propagators need to be redefined as in Eq. (4). The procedure for Diagram Removal 2 is similar to Wt for tWH production. This process is not studied in this note, but is explored in detail in Ref. [44].

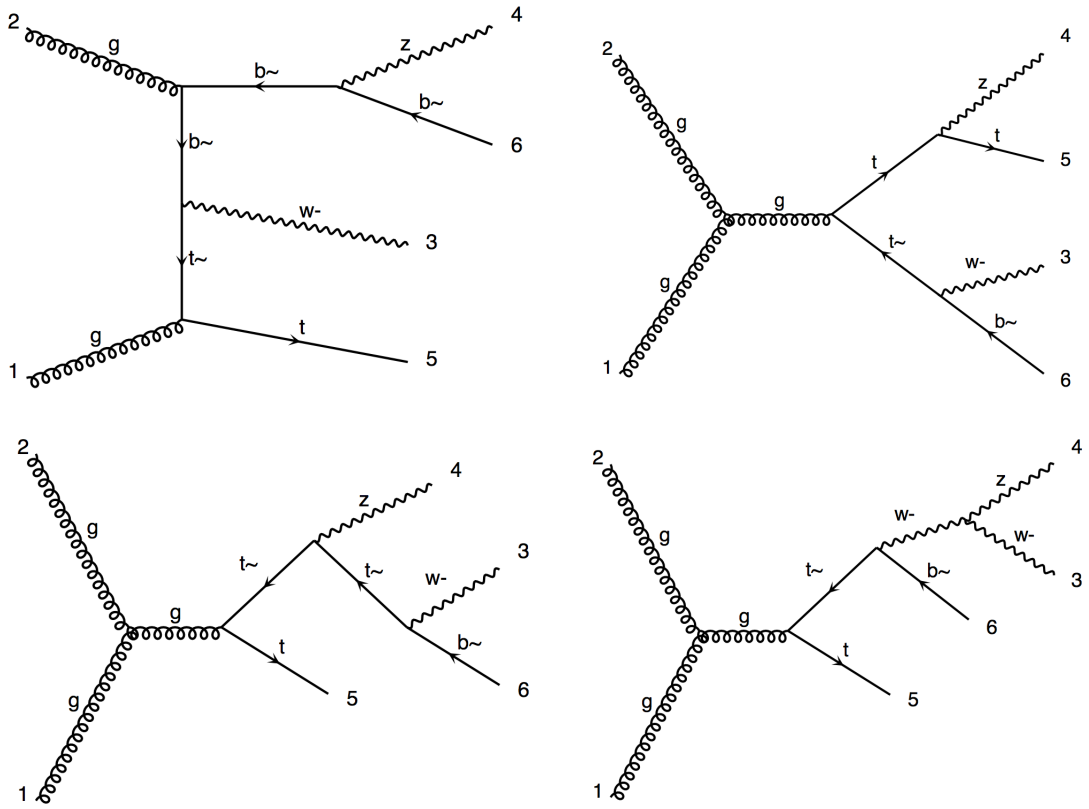

Figure 24: Diagrams generated [21] for tWZ production at NLO in the five flavour scheme, with a singly-resonant tWZ diagram at the top left. The top right and bottom left diagrams overlap with $t\bar{t}Z$ production at LO and the one to the bottom left overlaps with $t\bar{t}$ production, followed by the rare decay $\bar{t} \rightarrow W^- \bar{b} Z$. The bottom right diagram contains two top quark propagators that need to be regularised.

By construction, the difference between DR1 and DR2 should give the interference. However, in order to support this claim, one should check for the process in question whether DR2 or DR1 gives a result that is closer to a gauge invariant prediction. In Ref. [44], such computations are performed, testing theoretical motivations of the DR1, DR2 and DS predictions. DR2 is found to perform better than DR1 for the Wt and tWH processes.

All calculations and predictions in this section are performed for proton–proton collisions at a collision energy of $\sqrt{s} = 13$ TeV at NLO in QCD in the five-flavour scheme. For the case of the four-flavour scheme, the overlap would occur already at LO. In this part of note, the method is presented in an experimental context, with comparisons in fiducial regions between DR2 and more established methods.

3.1 Study of Wt distributions

In this part, the Diagram Removal 1 and 2 procedures are implemented for Wt production in MG5_aMC@NLO 2.3.2.2 and interfaced with MadSpin [24, 45] for particle decays and with Herwig++ 2.7.1 for parton shower. The PDF set for the matrix element is CT10 [46], the PDF set for the shower is CTEQ6L1 [16] and the UE-EE-5 set of tuned parameters [18] is employed for the underlying event. The predictions are compared with the nominal ATLAS sample for Wt production, produced with Powheg-Box r2856 and interfaced with Pythia6.428, which implements Diagram Removal 1. The PDF set for matrix-element generation for the nominal sample is CT10PDF and the CTEQ6L1 set together with the Perugia2012 tune [14] is used for the parton shower. A similar sample, with Diagram Subtraction implemented in Powheg-Box r2819, is also included below for comparison. The cross sections for the four samples are shown in Table 4. The total cross section differs by 10 % bewteen the DR1 and DR2 predictions in MG5_aMC@NLO and by 5 % for the DR1 and DS samples in Powheg-Box. The interference between Wt and $t\bar{t}$ is negative.

Method	Total cross section	Difference w.r.t. DR1
MG5_aMC@NLO DR1	7.87 pb	
MG5_aMC@NLO DR2	7.09 pb	-10 %
Powheg-Box DR1	7.16 pb	
Powheg-Box DS	6.82 pb	-5 %

Table 4: Cross sections for the dilepton samples produced with MG5_aMC@NLO (DR1, DR2) and with Powheg. In MG5_aMC@NLO, the DR2 prediction is 10 % lower than the one from DR1. In Powheg, the DS prediction is 5 % lower than the nominal DR1 prediction.

A fiducial region is defined by requiring exactly two leptons (electron or muon), defined to have p_{T} above 20 GeV and $|\eta| < 2.5$. The jets shown below have requirements of $p_{\mathrm{T}} > 25$ GeV and $|\eta| < 2.5$. These kinematic requirements are similar to those use at reconstructed level in a recent Wt cross-section measurement at 13 TeV [47]. The ratios at the bottom of Figs. 25, 26 and 27 are computed with respect to the nominal DR1 prediction from Powheg. The overflow is always included in the last bin.

In Fig. 25 the p_{T} of jets is shown. While the four predictions agree at low jet p_{T}, at higher p_{T} the two methods that include the interference (DR2, DS) are lower than the two DR1 predictions. This may indicate a larger interference with $t\bar{t}$ in topologies with jets of high p_{T}. Where only the leading jet is considered, the agreement between the two Powheg and the two MG5_aMC@NLO samples is better at low p_{T}.

Jet multiplicity and the pseudorapidity $|\eta|$ of the jet with the highest p_{T} are examined in Fig. 26. For the jet multiplicity, after the three jets bin, the DS and DR2 predictions decrease noticeably with respect to the two DR1 predictions. This corresponds to a higher interference with $t\bar{t}$ at higher jet multiplicity. This effect is larger for the DR2 with MG5_aMC@NLO than for DS with Powheg-Box. No clear pattern in the difference of shape is observed for the pseudorapidity of the leading jet.

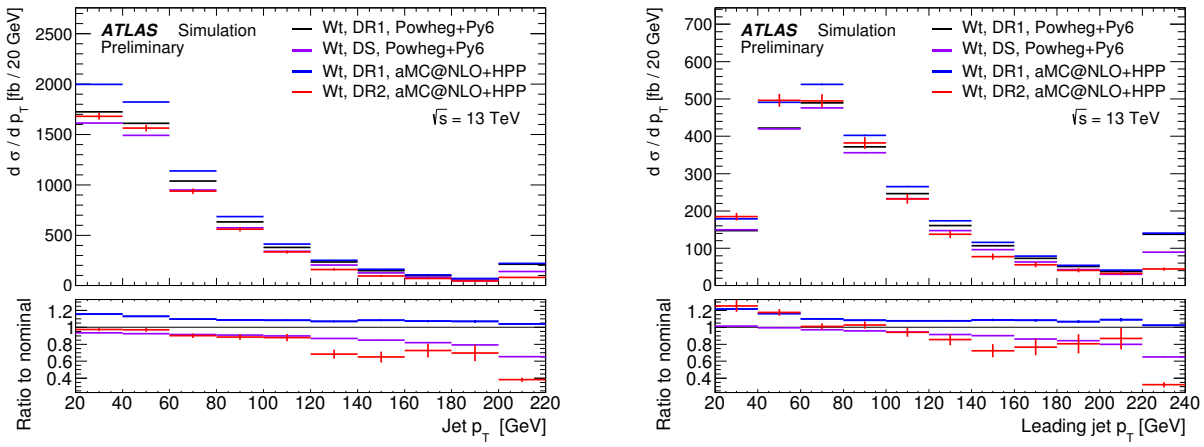

Figure 25: The distribution of p_{T} for all jets (left) and the leading jet (right) for Wt production with dileptonic decays, shown in a fiducial region. The nominal DR1 Powheg-Box prediction is shown in black, the Powheg-Box DS prediction in purple, the MG5_aMC@NLO DR1 in blue and the MG5_aMC@NLO DR2 in red. The ratio is computed with respect to the nominal distribution from Powheg-Box

.

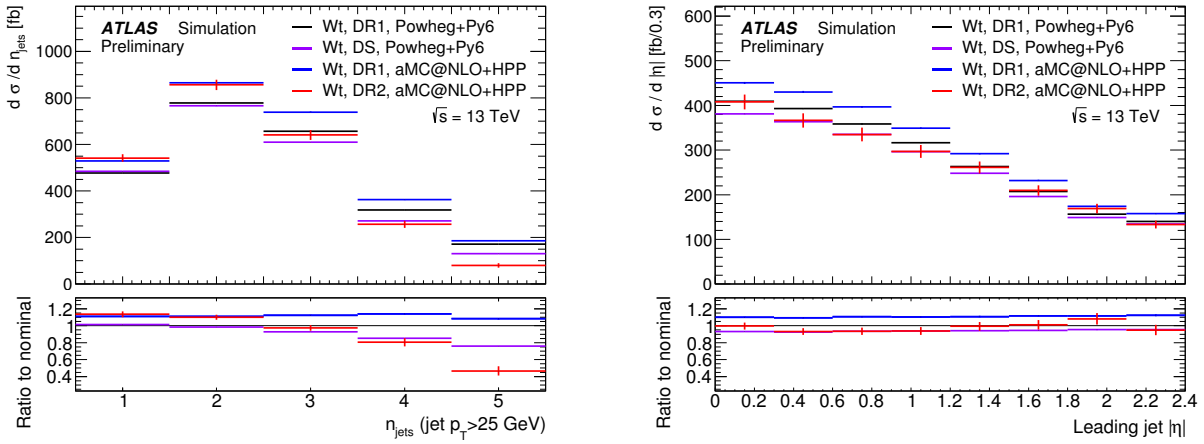

Figure 26: Jet multiplicity (left) and pseudorapidity of the jet with the highest transverse momentum (right) for Wt production with dileptonic decays, shown in a fiducial region. The nominal DR1 Powheg-Box prediction is shown in black, the Powheg-Box DS prediction in purple, the MG5_aMC@NLO DR1 in blue and the MG5_aMC@NLO DR2 in red. The ratio is computed with respect to the nominal distribution from Powheg-Box.

Figure 27 shows the p_{T} for electrons and for muons. The DS and DR2 predictions agree better with the nominal Powheg DR1 than the MG5_aMC@NLO DR1 prediction until around $p_{\mathrm{T}} = 100\,\mathrm{GeV}$. At higher p_{T}, the predictions that include the interference are lower than the DR1 predictions.

3.2 Study of tWZ distributions

In this part, the associated production of a Z boson with Wt is examined. This process is not currently measured at the LHC due to the combination of low production cross section and high background from $t\bar{t}Z$. Conversely, tWZ forms a major background in signal regions targeting $t\bar{t}Z$.

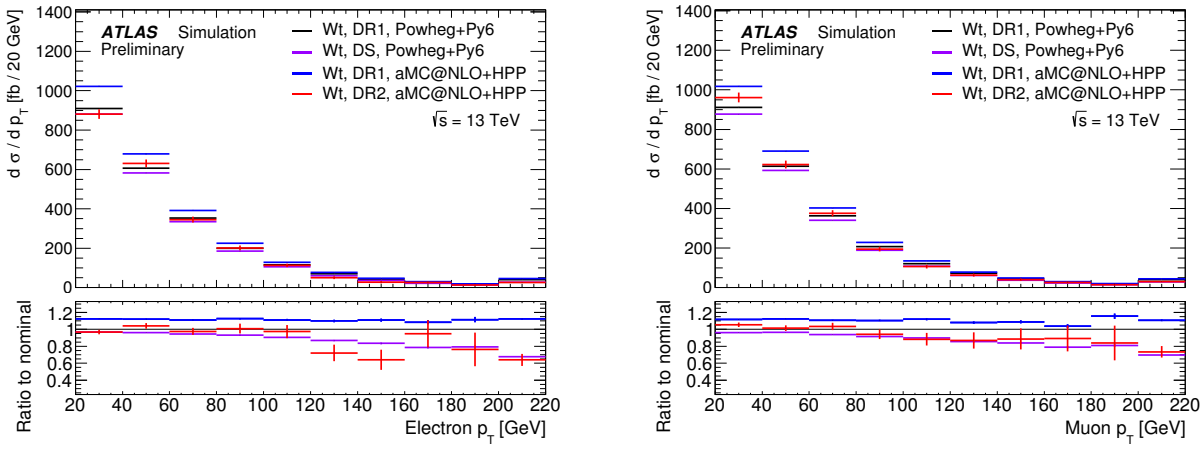

Figure 27: Electron p_{T} (left) and muon p_{T} (right), Wt production with leptonic decays for Wt production with dileptonic decays, shown in a fiducial region. The nominal DR1 Powheg-Box prediction is shown in black, the Powheg-Box DS prediction in purple, the MG5_aMC@NLO DR1 in blue and the MG5_aMC@NLO DR2 in red. The ratio is computed with respect to the nominal distribution from Powheg-Box.

For the event generation, MG5_aMC@NLO 2.3.2.2 is used to generate DR1 and DR2 predictions, with the PDF set NNPDF3.0NLO. MadSpin is implemented for the particle decays and Pythia8 is applied for parton shower with the A14 tune and the NNPDF23LO PDF set. The Z boson is required to decay leptonically in MadSpin.

The cross sections for these two samples are listed for the two different Diagram Removal methods in Table 5. It is found that DR2 gives a 28 % lower cross section than the nominal DR1 sample. This could indicate a large negative interference with $t\bar{t}Z$, provided that it can be shown that DR2 prediction is better theoretically motivated than DR1. This difference in the predictions for tWZ is of similar magnitude for tWH, as shown in Ref. [44], where DR2 was found to give a prediction closer to the gauge invariant calculation at leading order.

For tWZ, more types of diagrams contribute to the interference than for Wt, which gives a larger relative difference in the predictions of DR1 and DR2. While Wt only has overlapping diagrams corresponding to the top-quark decay $t \to Wb$ (Fig. 23), for tWZ, there are also contributions from diagrams corresponding to the $t\bar{t}Z$-like channel that contains the chain $t \to tZ \to WbZ$ and what looks like $t\bar{t}$ production followed by a rare top-quark decay $t \to bW \to bWZ$ (see Fig. 24). It should also be pointed out that at the level of the matrix-element generation, the difference between DR2 and DR1 is -22% rather than the -28% found based on truth studies (with the Pythia8 shower applied together with the A14 tune). Using the A14 tune could affect the DR1 and DR2 predictions differently, as these have differences in shape for distributions such as p_{T} of the Z boson (see Fig. 28). The differences between the A14 tune and data is shown for this distribution in Ref. [18].

Currently, the DR1 prediction for tWZ is used as the nominal background sample for the $t\bar{t}Z$ measurement [48], while the total difference from the DR2 prediction on the matrix-element level (-22%) is used to evaluate the normalisation uncertainty on tWZ.

In Figs. 28–30, different distributions for the tWZ process are shown in Figs. 28–30. At least three jets are required with p_{T} above 25 GeV and $|\eta| < 2.5$ and at least two leptons above 15 GeV and with $|\eta| < 2.5$.

Method	Cross section	Difference w.r.t. DR1
MG5_aMC@NLO DR1	15.6 fb	
MG5_aMC@NLO DR2	12.2 fb	-28%

Table 5: The inclusive cross sections for the tWZ samples, assessed with DR1 and DR2 in MG5_aMC@NLO and interfaced with PYTHIA8. The Z boson is required to decay leptonically. The DR2 prediction is 28% lower than DR1.

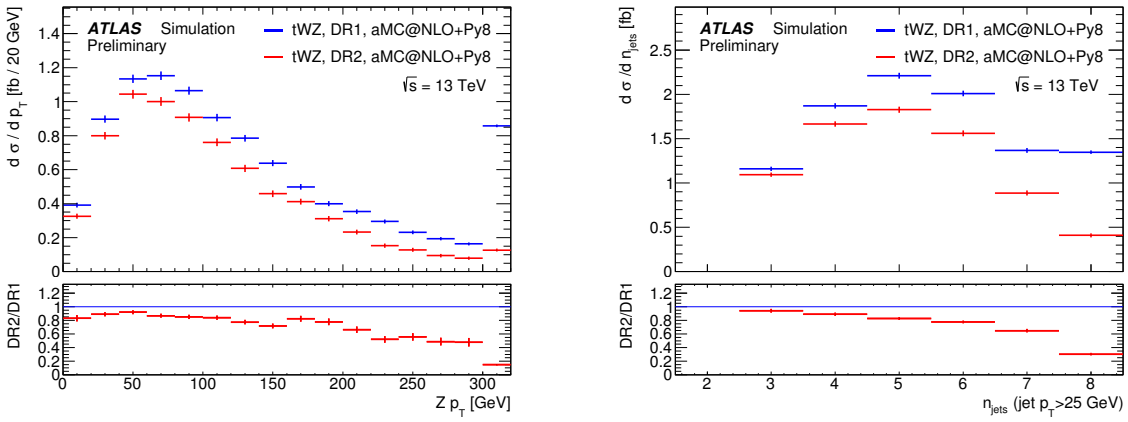

Figure 28: Z-boson p_T (left) and jet multiplicity (right) for tWZ production with leptonic Z decays, shown in a fiducial region. The Z boson is required to originate from the hard scattering process. The nominal prediction from MG5_aMC@NLO with DR1 is shown in blue and the MG5_aMC@NLO DR2 in red. The ratio is computed with respect to the DR1 prediction.

These cuts are applied on the truth level to approach the signal regions on reconstructed level for the $t\bar{t}Z$ measurements [48, 49].

One distribution that shows a prominent difference between the DR1 and DR2 predictions is the p_{T} of the Z boson from the hard process, Fig. 28. The Z-boson p_{T} steadily decreases for the DR2 compared to DR1, even more so above 200 GeV. Above 300 GeV (in the overflow bin), it amounts to less than 20 % of the DR1 prediction. In the same figure, the jet multiplicity is shown, with the differences in predictions increasing with jet multiplicity. As $t\bar{t}Z$ production tends to result in more jets than tWZ, the negative interference is expected to grow with jet multiplicity.

In Fig. 29, the p_{T} of jets and of the leading jets is shown. At high jet p_{T}, the differences between the predictions is large, in particular when only the jet with the highest p_{T} is considered. Finally, in Fig. 30, the p_{T} of leptons is shown. Similarly to Z p_{T}, the difference between the predictions increases with p_{T}, but the trend is weaker.

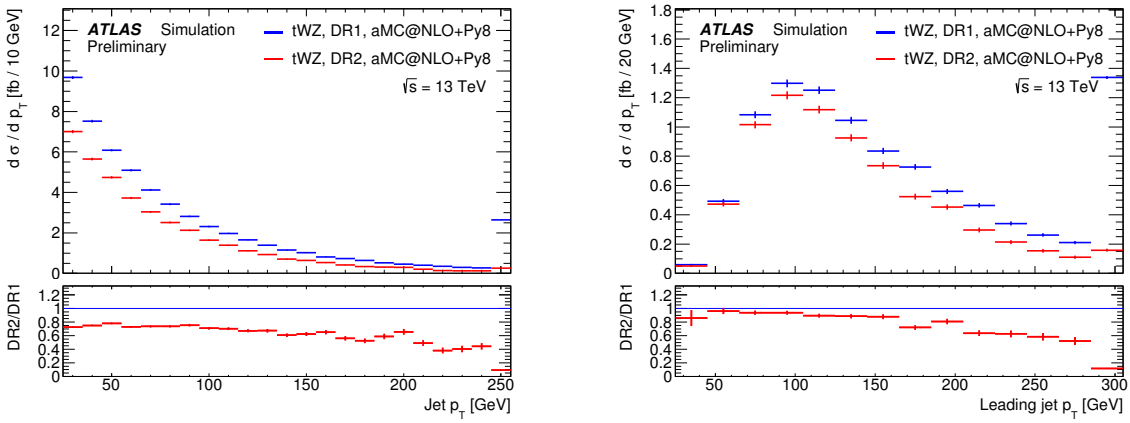

Figure 29: Jet p_T (left) and leading jet p_{T} (right) for tWZ production with leptonic Z decays, shown in a fiducial region. The nominal prediction from MG5_aMC@NLO with DR1 is shown in blue and the MG5_aMC@NLO DR2 in red. The ratio is computed with respect to the DR1 prediction.

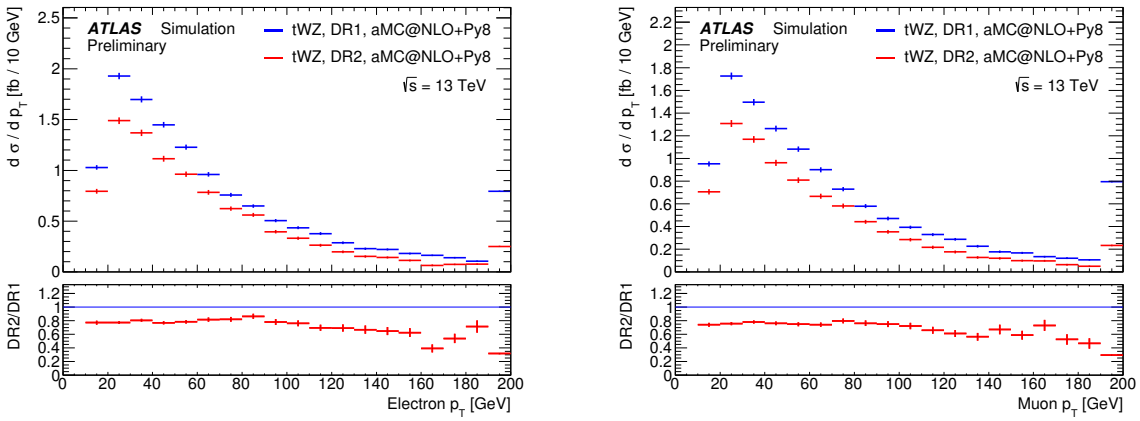

Figure 30: Electron p_T (left) and muon p_T (right) for tWZ production with leptonic Z decays, shown in a fiducial region. The nominal prediction from MG5_aMC@NLO with DR1 is shown in blue and the MG5_aMC@NLO DR2 in red. The ratio is computed with respect to the DR1 prediction.

3.3 Summary and discussion

A new implementation of Diagram Removal can be employed in MG5_aMC@NLO to remove the overlaps for Wt-like processes. From the theory point of view, the main advantage of the method is being able to include the interference with $t\bar{t}$-like processes without relying on momentum reshuffling. In this note, Diagram Removal 2 is applied to the Wt and tWZ in regions similar to signal regions for measurements of Wt and $t\bar{t}Z$ processes, with tWZ forming a major background for the latter. This is the first time that the mehod is implemented for tWZ. The difference between DR1 and DR2 predictions can be used to assess the effect of the interference.

While there is an overall cross-section difference between DR1 and DR2 with MG5_aMC@NLO, the predicted shapes agree at low p_{T} of jets and leptons but start to diverge at higher p_{T}. In tWZ, the interference is larger and the shapes are more distinct. Diagram Removal is more complicated for tWZ than for tW and tWH, since interference from $t\bar{t}$ production followed by rare top-quark decay ($t \to WbZ$) also interferes with tWZ. The contribution and behaviour of this subprocess should be investigated to understand tWZ better.

For the future, it would be interesting to improve both the DR1 and DR2 predictions in MG5_aMC@NLO, interfaced with MadSpin, by following an analogous Diagram Removal procedure in MadSpin, as has been recently proposed by the authors of Ref. [44]. This could be important for analyses where spin properties are studied.

In summary, there is more to understand about overlap removal schemes for the Wt, tWZ and tWH processes than was considered previously and this should be taken into account when modelling them, both when they enter as either signal or background. Comparisons with data would be useful to evaluate the overlap removal methods for Wt, together with forming a better theoretical understanding, as investigated in Ref. [44]. A better way to handle the $t\bar{t}$-Wt interference in MC is to generate this as a single sample using the $WbWb$ final state at NLO precision. This process has recently become available in Powheg-Box [50]. For tWZ, more detailed theoretical studies are needed to understand the process.

4 Conclusions

The Monte Carlo simulation setup for top-quark pair production has been studied for the modelling of the Powheg generator interfaced to the Pythia8 and Herwig7 shower generators. Using unfolded data from ATLAS analyses at $\sqrt{s} = 8\,\mathrm{TeV}$ and $\sqrt{s} = 13\,\mathrm{TeV}$ optimal modelling using $h_{\mathrm{damp}} = 1.5 \cdot m_{\mathrm{top}}$ has been found. All relevant distributions are in agreement within experimental uncertainties for Powheg+Pythia8 using the A14 set of tuned parameters. The Powheg+Herwig7 shows the best modelling using the `Colour3` reconstruction option; in particular the p_{T} of the top quark agrees well with the unfolded data distribution. However, the jet multiplicity is not well described and further studies are need. Finally a new method to take into account interference effects between Wt single-top-quark production and $t\bar{t}$ production has been studied and compared with established methods.

References

[1] ATLAS Collaboration, *Comparison of Monte Carlo generator predictions to ATLAS measurements of top pair production at 7 TeV*, ATL-PHYS-PUB-2015-002, 2015, URL: http://cds.cern.ch/record/1981319.

[2] ATLAS Collaboration, *Simulation of top-quark production for the ATLAS experiment at $\sqrt{s}$ = 13 TeV*, ATL-PHYS-PUB-2016-004, 2016, URL: http://cds.cern.ch/record/2120417.

[3] ATLAS Collaboration, *Further studies on simulation of top-quark production for the ATLAS experiment at $\sqrt{s}$ = 13 TeV*, ATL-PHYS-PUB-2016-016, 2016, URL: http://cds.cern.ch/record/2205262.

[4] M. Beneke et al., *Hadronic top-quark pair production with NNLL threshold resummation*, Nucl. Phys. B **855** (2012) 695, arXiv: 1109.1536 [hep-ph].

[5] M. Cacciari et al., *Top-pair production at hadron colliders with next-to-next-to-leading logarithmic soft-gluon resummation*, Phys. Lett. B **710** (2012) 612, arXiv: 1111.5869 [hep-ph].

[6] P. Bärnreuther, M. Czakon and A. Mitov, *Percent Level Precision Physics at the Tevatron: First Genuine NNLO QCD Corrections to $q\bar{q} \to t\bar{t} + X$*, Phys. Rev. Lett. **109** (2012) 132001, arXiv: 1204.5201 [hep-ph].

[7] M. Czakon and A. Mitov, *NNLO corrections to top-pair production at hadron colliders: the all-fermionic scattering channels*, JHEP **1212** (2012) 054, arXiv: 1207.0236 [hep-ph].

[8] M. Czakon and A. Mitov, *NNLO corrections to top pair production at hadron colliders: the quark-gluon reaction*, JHEP **1301** (2013) 080, arXiv: 1210.6832 [hep-ph].

[9] M. Czakon, P. Fiedler and A. Mitov, *The total top quark pair production cross-section at hadron colliders through $O(\alpha_S^4)$*, Phys. Rev. Lett. **110** (2013) 252004, arXiv: 1303.6254 [hep-ph].

[10] M. Czakon and A. Mitov, *Top++: A Program for the Calculation of the Top-Pair Cross-Section at Hadron Colliders*, Comput. Phys. Commun. **185** (2014) 2930, arXiv: 1112.5675 [hep-ph].

[11] S. Frixione et al., *A positive-weight next-to-leading-order Monte Carlo for heavy flavour hadro-production*, JHEP **0709** (2007) 126, arXiv: 0707.3088 [hep-ph].

[12] P. Nason, *A New method for combining NLO QCD with shower Monte Carlo algorithms*, JHEP **0411** (2004) 040, arXiv: hep-ph/0409146.

[13] T. Sjöstrand, S. Mrenna and P. Z. Skands, *PYTHIA 6.4 Physics and Manual*, JHEP **0605** (2006) 026, arXiv: hep-ph/0603175.

[14] P. Z. Skands, *Tuning Monte Carlo Generators: The Perugia Tunes*, Phys. Rev. D **82** (2010) 074018, arXiv: 1005.3457 [hep-ph].

[15] H.-L. Lai et al., *New parton distributions for collider physics*, Phys. Rev. D **82** (2010) 074024, arXiv: 1007.2241 [hep-ph].

[16] J. Pumplin et al., *New Generation of Parton Distributions with Uncertainties From Global QCD Analysis*, JHEP **0207** (2002) 012, arXiv: hep-ph/0201195.

[17] T. Sjöstrand et al., *An Introduction to PYTHIA 8.2*, Comput. Phys. Commun. **191** (2015) 159, arXiv: 1410.3012 [hep-ph].

[18] ATLAS Collaboration, *ATLAS Pythia 8 tunes to 7 TeV data*, ATL-PHYS-PUB-2014-021, 2014, URL: http://cds.cern.ch/record/1966419.

[19] M. Bahr et al., *Herwig++ Physics and Manual*, Eur. Phys. J. C **58** (2008) 639, arXiv: 0803.0883 [hep-ph].

[20] J. Bellm et al., *Herwig 7.0/Herwig++ 3.0 release note*, Eur. Phys. J. C **76** (2016) 196, arXiv: 1512.01178 [hep-ph].

[21] J. Alwall et al., *The automated computation of tree-level and next-to-leading order differential cross sections, and their matching to parton shower simulations*, JHEP **1407** (2014) 079, arXiv: 1405.0301 [hep-ph].

[22] R. D. Ball et al., *Parton distributions with LHC data*, Nucl. Phys. B **867** (2013) 244, arXiv: 1207.1303 [hep-ph].

[23] NNPDF Collaboration, R.D. Ball et al., *Parton distributions for the LHC Run II*, JHEP **1504** (2015) 040, arXiv: 1410.8849 [hep-ph].

[24] P. Artoisenet et al., *Automatic spin-entangled decays of heavy resonances in Monte Carlo simulations*, JHEP **1303** (2013) 015, arXiv: 1212.3460 [hep-ph].

[25] T. Gleisberg et al., *Event generation with SHERPA 1.1*, JHEP **0902** (2009) 007, arXiv: 0811.4622 [hep-ph].

[26] S. Höche et al., *QCD matrix elements + parton showers: The NLO case*, JHEP **1304** (2013) 027, arXiv: 1207.5030 [hep-ph].

[27] R. Frederix and S. Frixione, *Merging meets matching in MC@NLO*, JHEP **1212** (2012) 061, arXiv: 1209.6215 [hep-ph].

[28] A. Buckley et al., *Rivet user manual*, Comput. Phys. Commun. **184** (2013) 2803, arXiv: 1003.0694 [hep-ph].

[29] ATLAS Collaboration, *Measurements of top-quark pair differential cross-sections in the lepton+jets channel in pp collisions at $\sqrt{s}$ = 8 TeV using the ATLAS detector*, (2015), arXiv: 1511.04716 [hep-ex].

[30] M. Cacciari and G. P. Salam, *Pileup subtraction using jet areas*, Phys. Lett. B **659** (2008) 119, arXiv: 0707.1378 [hep-ph].

[31] M. Cacciari, G. P. Salam and G. Soyez, *The Catchment Area of Jets*, JHEP **0804** (2008) 005, arXiv: 0802.1188 [hep-ph].

[32] ATLAS Collaboration, *Performance of jet substructure techniques for large-R jets in proton–proton collisions at $\sqrt{s}$ = 7 TeV using the ATLAS detector*, JHEP **09** (2013) 076, arXiv: 1306.4945 [hep-ex].

[33] M. Cacciari, G. P. Salam and G. Soyez, *The anti-k_t jet clustering algorithm*, JHEP **0804** (2008) 063, arXiv: 0802.1189 [hep-ph].

[34] ATLAS Collaboration, *Measurement of the differential cross-section of highly boosted top quarks as a function of their transverse momentum in $\sqrt{s}$ = 8 TeV proton–proton collisions using the ATLAS detector*, Phys. Rev. D **93** (2016) 032009, arXiv: 1510.03818 [hep-ex].

[35] ATLAS Collaboration, *Measurements of top-quark pair differential cross-sections in the lepton+jets channel in pp collisions at $\sqrt{s}$ = 13 TeV using the ATLAS detector*, ATLAS-CONF-2016-040, 2016, URL: http://cds.cern.ch/record/2206075.

[36] ATLAS Collaboration, *Measurements of normalized differential cross-sections for $t\bar{t}$ production in pp collisions at $\sqrt{s}$ = 7 TeV using the ATLAS detector*, Phys. Rev. D **90** (2014) 072004, arXiv: 1407.0371 [hep-ex].

[37] ATLAS Collaboration, *Measurement of the $t\bar{t}$ production cross-section as a function of jet multiplicity and jet transverse momentum in 7 TeV proton–proton collisions with the ATLAS detector*, JHEP **01** (2015) 020, arXiv: 1407.0891 [hep-ex].

[38] ATLAS Collaboration, *Measurements of fiducial cross-sections for $t\bar{t}$ production with one or two additional b-jets in pp collisions at $\sqrt{s}$ = 8 TeV using the ATLAS detector*, Eur. Phys. J. C **76** (2016) 11, arXiv: 1508.06868 [hep-ex].

[39] A. Buckley and D. Bakshi Gupta, *Powheg-Pythia matching scheme effects in NLO simulation of dijet events*, 2016, arXiv: 1608.03577 [hep-ph].

[40] T. Sjöstrand, 'Pythia8.2 online manual: Powheg Merging', URL: http://home.thep.lu.se/~torbjorn/pythia82html/POWHEGMerging.html.

[41] ATLAS Collaboration, *Search for New Phenomena in Dijet Angular Distributions in Proton–Proton Collisions at $\sqrt{s}$ = 8 TeV Measured with the ATLAS Detector*, Phys. Rev. Lett. **114** (2015) 221802, arXiv: 1504.00357 [hep-ex].

[42] S. Frixione et al., *Single-top hadroproduction in association with a W boson*, JHEP **0807** (2008) 029, arXiv: 0805.3067 [hep-ph].

[43] E. Re, *Single-top Wt-channel production matched with parton showers using the POWHEG method*, Eur. Phys. J. C **71** (2011) 1547, arXiv: 1009.2450 [hep-ph].

[44] F. Demartin et al., *tWH associated production at the LHC*, 2016, arXiv: 1607.05862 [hep-ph].

[45] S. Frixione et al., *Angular correlations of lepton pairs from vector boson and top quark decays in Monte Carlo simulations*, JHEP **0704** (2007) 081, arXiv: hep-ph/0702198.

[46] M. Guzzi et al., *CT10 parton distributions and other developments in the global QCD analysis*, 2011, arXiv: 1101.0561 [hep-ph].

[47] ATLAS Collaboration, *Measurement of the cross-section of the production of a W boson in association with a single top quark with ATLAS at $\sqrt{s}$ = 13 TeV*, ATLAS-CONF-2016-065, 2016, URL: https://cds.cern.ch/record/2206207.

[48] ATLAS Collaboration, *Measurement of the $t\bar{t}Z$ and $t\bar{t}W$ production cross sections in multilepton final states using 3.2 fb^{-1} of pp collisions at $\sqrt{s}$ = 13 TeV with the ATLAS detector*, 2016, arXiv: 1609.01599 [hep-ex].

[49] ATLAS Collaboration, *Measurement of the $t\bar{t}W$ and $t\bar{t}Z$ production cross sections in pp collisions at $\sqrt{s}$ = 8 TeV with the ATLAS detector*, JHEP **1511** (2015) 172, arXiv: 1509.05276 [hep-ex].

[50] T. Ježo et al., *An NLO+PS generator for $t\bar{t}$ and Wt production and decay including non-resonant and interference effects*, 2016, arXiv: 1607.04538 [hep-ph].